Design and Construction of a Fast Neutron Irradiation Facility for Use at Elevated Temperature

by

Robertus Ismuntoyo

Doktorandus of Physics
Gadjah Mada University, 1967
INDONESIA

A MASTER'S THESIS

submitted in partial fulfillment of the
requirement for the degree

Department of Nuclear Engineering
Kansas State University
Manhattan, Kansas 66506

1981

Approved by:

Joseph F. Merklin
Major Professor

TABLE OF CONTENTS

LIST OF TABLES AND FIGURES

Appendix Figures

ACKNOWLEDGMENTS

I wish to thank the Department of Nuclear Engineering and the International Atomic Energy Agency for the financial support provided during the completion of this work.

I also appreciate the support and guidance of the Faculty of the Department of Nuclear Engineering, particularly Dr. J. F. Merklin. Also, to Mr. William Starr and Mrs. M. Brisbin for their help in many areas, I extend many thanks.

1.0 INTRODUCTION

A research reactor is an important tool in the area of Nuclear Science and Technology. Some of the research reactors are specifically designed to be used in a particular field, such as the JANUS Reactor which was designed for biological and medical research.[1] Others are designed to be multi-purpose reactors, such as the TRIGA Reactor type or Swimming Pool Research Reactor. For multi-purpose research reactors, they are usually designed to provide irradiation facilities inside and surrounding the core, and also to provide beams of neutrons by means of beamports. The first two generations of TRIGA reactor type, Mark I and II, provide 40 irradiation channels in the reflector surrounding the core, called the rotary specimen rack, and one irradiation facility in the center of the core. The Mark I is not equipped with beamports, but Mark II has four beamports which are capable of irradiating a specimen up to a diameter of 15 cm.

The utilization of a research reactor to study radiation damage of materials was initiated shortly after the Second World War. Most of the studies were concentrated to support the development of power reactors. Since conditions in a power reactor are different than in a research reactor, such as temperature and pressure, special irradiation facilities must be installed in a research reactor. Some of the irradiation facilities were designed to simulate the temperature in a power reactor, such as the TRIGA King Furnace for the TRIGA Mark I and II reactors[2]. The furnace has the dimensions of a standard TRIGA fuel element, so it can be placed anywhere inside the core. The

chamber can be operated up to 2000 K for steady state operation, or 3300 K for pulsed operation. The heater is made from graphite, and helium can be used as a purge gas. The material testing reactors are a more advanced type of research reactors, they have the ability to irradiate the sample with the same neutron density as in a power reactor, or sometimes higher. Experiments can be performed at higher temperatures and pressures than the normal conditions in a power reactor, using a special irradiation rig. The irradiation facility for this type of reactor can study the characteristics of a fuel rod for a power reactor. Sometimes a test for a whole fuel bundle for a power reactor has to be done, in this case a small research reactor or a material testing reactor cannot provide the space and/or the neutron density. For this purpose, the advanced material testing reactor and the engineering test reactor are used.[1]

In this work the main objective is to install an irradiation chamber, that can operate from room temperature up to approximately 1000 K, and that the chamber is exposed to a fast neutron flux with minimal amount of thermal neutrons and gamma rays. With these requirements, location in a beamport presents the least difficulties. Location inside the reactor core will present too many disadvantages. First, the undesirable gamma exposure will be too high, approximately 10^4 rad/sec at the core surface.[3] Secondly is the difficulty to reduce the thermal neutron flux. If, for instance, a cadmium sheet is used, then the operating temperature of the chamber must be lower than the melting point of cadmium metal, which is 322°C.[4] Other thermal neutron absorbing materials would have to be specially machined or the absorption

cross section of other absorbing material is not large enough. Therefore, the absorber must be very thick. The thermal neutron absorber also causes a negative reactivity to the reactor. Third, the effective size of the specimen chamber will be very small, without a special kind of heater. There are other reasons, such as the difficulty in inserting and removing the sample, and the space, available for measuring temperature and other experimental parameters, is very limited.

The next step is to choose which one of the beam ports is the most appropriate to match the design requirements. The detailed explanation for the beamport selection will be given in the next section.

In order to evaluate the radiation chamber and to meet the safety requirements, four tests were conducted. The first test is related to the safety of the reactor, which is the temperature distribution in the surrounding area of the heater, especially the maximum temperature in the beamport liner. Before actual testing in the beamport, preliminary tests in the beam plug storage hole were done. This storage hole has similar size and composition as the beamport itself. A direct temperature measurement on the storage liner is possible, because the storage hole was designed to accomodate the inner beamport plug only. From the result of this measurement, the correlation of the temperatures between the outer tube of the chamber and the beam plug storage liner can be determined. Hence, if the temperature on the hot spot of the outer tube is monitored continuously, then the approximate temperature on the beam-port liner can be predicted. The second test was concerned with the radiological hazard in the surrounding areas of the beamport. This is necessary, since, during the operation of the

heater, the temperature on the outer tube and the purge gas flow must be kept within certain limits. This entails that the operator must work approximately 2 meters on the side of the beamport during the irradiation. The third test is the measurement of both thermal and fast neutron flux, before and after the installation of the radiation chamber. The thermal neutron flux was measured using gold foils. The fast neutron flux was measured using threshold detectors, which were In, Ni, and Al. With these three detectors, the fast neutron spectrum can be measured for the intervals, 1.4-2.7, 2.7-7.1, and 7.1-20 MeV. The fourth test was the irradiation of LiF in the irradiation chamber. The first set of irradiations was done at room temperature with fluences from 5×10^{13} up to 4×10^{14} cm^{-2} sec^{-1}. Then the sample temperature was varied from room temperature up to 700 K. The second set was the gamma irradiation of LiF in the Gamma-cell Irradiator, the result of this irradiation was used to approximate the effect of the fission gamma rays during the irradiation in the chamber. Then the effect due to fast neutron is the difference between the result of irradiation in the chamber and the change due to the gamma irradiation.

2.0 DESCRIPTION OF REACTOR[5]

The Kansas State University reactor is a research reactor made by General Atomic Inc. The Reactor is a TRIGA Mark II type, in which 20% enriched uranium is mixed with Zirconium Hydride. With this composition the TRIGA reactor is classified as a solid homogeneous reactor. The cooling is provided with water by natural convection. It has a nominal power of 250 kW, and the ability to pulse up to 250 MW at peak power or maximum reactivity insertion of $2.00. The reactor was commissioned on October 16, 1962, with maximum power 100 kW.[6] Then on July 31, 1968, the reactor was allowed to operate continuously with maximum power 250 kW and also for pulse mode operation with peak power 250 MW or insertion of positive reactivity up to $2.00.[7] Excluding the positions for three control rods, central thimble, neutron source, and two experimental positions, the core has 86 channels for fuel elements. At the present time, the core has 79 fuel elements.

The overall view of the reactor is shown in Fig. 1. The reactor is furnished with four beam ports, one thermal column, one thermalizing column which is located between the reactor tank and the bulk shielding facility, a rotary speciment rack which has 40 channels for irradiation, one irradiation facility in the center of the core, and one pneumatic transfer irradiation facility at ring F. The four beam ports penetrate the concrete shield and the aluminum tank to the reflector. The beam-port liner was made stepwise to prevent radiation streaming. The liner closest to the core, has a diameter of 15.2 cm, and is made from aluminum.

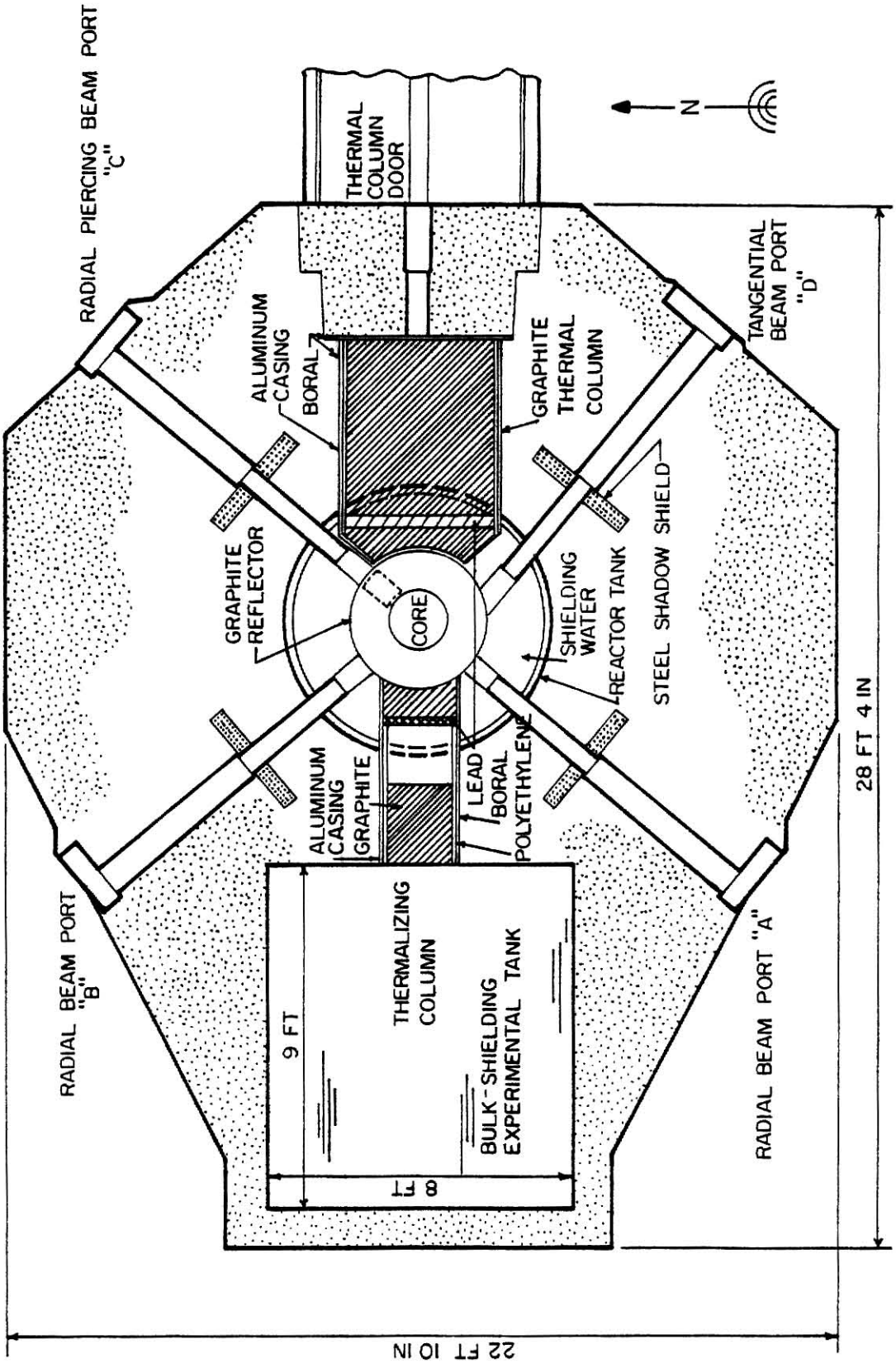

Fig. 1. Reactor Layout

Then the liner diameter is increased stepwise with a nominal inner diameter of 20.3 cm at the outer surface of the concrete shield. The larger liner was made from steel plated with cadmium to prevent corrosion. In case that the beamports are not used, a special shielding is provided along the axis of the beam tube to reduce the radiation outside the concrete shield to a safe level. This special shielding is composed of four parts, i.e., a concrete plug contained in an aluminum structure for the liner close to the core, a wooden plug for the larger liner, a lead-filled shutter, and a lead lined door.

The four beam ports provide irradiation facililities for large specimens, up to 15.2 cm in diameter. One of the beamports is aligned tangentially to the core, which terminates at the outer surface of the reflector. The other three are oriented radially with respect to the center of the core, and they are called radial beamports. Two of the radial beamports terminate at the outer edge of the reflector assembly, and the third is aligned with a cylindrical void in the graphite reflector. The void passes beneath the rotary specimen rack so that the horizontal center line of the beamport is located 7 cm below the centerline of the core. This radial beamport is called the radial piercing beamport to distinguish it from the other radial beamports.

3.0 DESCRIPTION OF THE IRRADIATION CHAMBER DESIGN

The objective of this work is to design, construct, and install an irradiation chamber so that samples can be exposed to a fast neutron field with a minimal thermal neutron flux and a minimal gamma ray flux, and so that the sample temperature can be varied from room temperature to 1000 K. The chamber must be equipped also with a purge gas to remove part of the heat, and to reduce the possibility of sample oxidation during irradiation at higher temperature. To meet the safety requirement for the concrete shielding and the radiation chamber, the temperature must be monitored in a number of positions in the chamber.

3.1 Choice of Beamport

As stated in Chapter 2, the KSU TRIGA Mark II reactor has four beamports. The tangential beamport, which is aligned in the southeast direction, has the lowest gamma flux, but also has the lowest fraction of fast neutrons, because the end of beamport is at the outer surface of the reflector. Hence, the tangential beamport does not fit for the location of the chamber.

The two radial beamports, which are aligned in the southwest and northwest directions, have higher fast neutron and gamma fluxes. But the fast neutron flux, compared to the fast neutron flux at the core surface, is reduced considerably. This is caused by the reflector, which is made of 30 cm of graphite. The average fast neutron energy is shifted to higher energy due to the moderation of

the lower part of fast neutron spectrum by the reflector. As shown in Fig. 1, these two radial beamports are beamports A and B, and the tangential beamport is beamport D.

The inner end of the radial piercing beamport is practically at the core surface. This means that the fast neutron spectrum, is similar to the spectrum at the core surface. This occurs, since inside the reflector, a hollow space is aligned with the axial direction of the radial piercing beamport. The only material between the core and the beamport is aluminum, and aluminum is a poor moderator.

For the above reasons, the radial piercing beamport is the best beamport when compared with the other beamports for the location of the irradiation chamber. The fast neutron energy spectrum is very similar to the spectrum at the core surface, and, the attenuation of the flux is due to the geometrical attenuation only. West,[8] in GA-4361, has calculated the neutron spectrum in the core and surrounding areas. The neutron flux at the core surface can be approximated with the flux at ring -F. Table 1 presents the values of the neutron flux in the four beamports and Table 2 presents the values for the fast neutron spectrum in ring -F.[8].

THIS BOOK CONTAINS NUMEROUS PAGES WITH THE ORIGINAL PRINTING BEING SKEWED DIFFERENTLY FROM THE TOP OF THE PAGE TO THE BOTTOM.

THIS IS AS RECEIVED FROM THE CUSTOMER.

Table 1. Neutron flux at the inner end of beamports[8].

Beamport	Thermal Neutron Flux* $\{cm^{-2}\ sec^{-1}\ watt^{-1}\}$	Fast Neutron Flux+ $\{cm^{-2}\ sec^{-1}\ watt^{-1}\}$
Tangential (S.E)	2.8×10^{6}	3.9×10^{5}
Radial (S.W)	2.8×10^{6}	3.9×10^{5}
Radial (N.W)	2.8×10^{6}	3.9×10^{5}
Radial Piercing (N.E)	1.3×10^{7}	2.5×10^{7}

*Thermal flux: Neutron with energy 0-1 eV.

+Fast flux: Neutron with energy 1 eV - 10 MeV.

Table 2. Fast neutron spectrum in Ring-F[8].

Energy Range {MeV}	Flux $\{cm^{-2}\ sec^{-1}\ watt^{-1}\}$	
	Fueled Ring-F	Unfueled Ring-F
1.35 - 2.23	0.206×10^{7}	0.170×10^{7}
2.23 - 3.68	0.164×10^{7}	0.135×10^{7}
3.68 - 4.72	0.0458×10^{7}	0.0367×10^{7}
4.72 - 6.07	0.0266×10^{7}	0.0218×10^{7}
6.07 - 7.79	0.0118×10^{7}	0.0096×10^{7}
7.79 - 10.0	0.0041×10^{7}	0.0033×10^{7}

3.2 The Design of the Irradiation Chamber

The irradiation chamber was designed in such a way so that it will provide a fast neutron field in the specimen chamber and then attenuate the residual thermal neutron, fast neutron, and the gamma fluxes to a safe level at the outlet of the beamport. The simplified diagram of the irradiation chamber inside the radial piercing beamport is shown in Fig. 2.

The chamber composed three major parts, these are the heater structure, the beamplug structure and the specimen holder. The heater structure provides a volume which can be heated to 900 K by a Nichrome wire heater. Surrounding the heater, two steel tubes were installed. These tubes are heated by convection and radiation and they transfer heat by conduction to the aluminum supporting disk (see Figs. 2 and 3). At the end of heater structure, facing the reactor core, a cadmium sheet was attached to absorb the thermal neutrons. The beamplug structure, which fits in the larger part of the beamport, was made from a steel tube. The tube was filled with borated paraffin and has 5 cm thick lead disk at both ends. In the center of the beamplug, a cadmium covered square aluminum channel was installed for insertion of the specimen holder. The heater structure was attached to the beamplug with the help of eight screws in the radial direction. The specimen holder was made from two materials, the section made from steel, and the other part was made from wood for neutron moderation. The detailed description of each structure is given in the following sections.

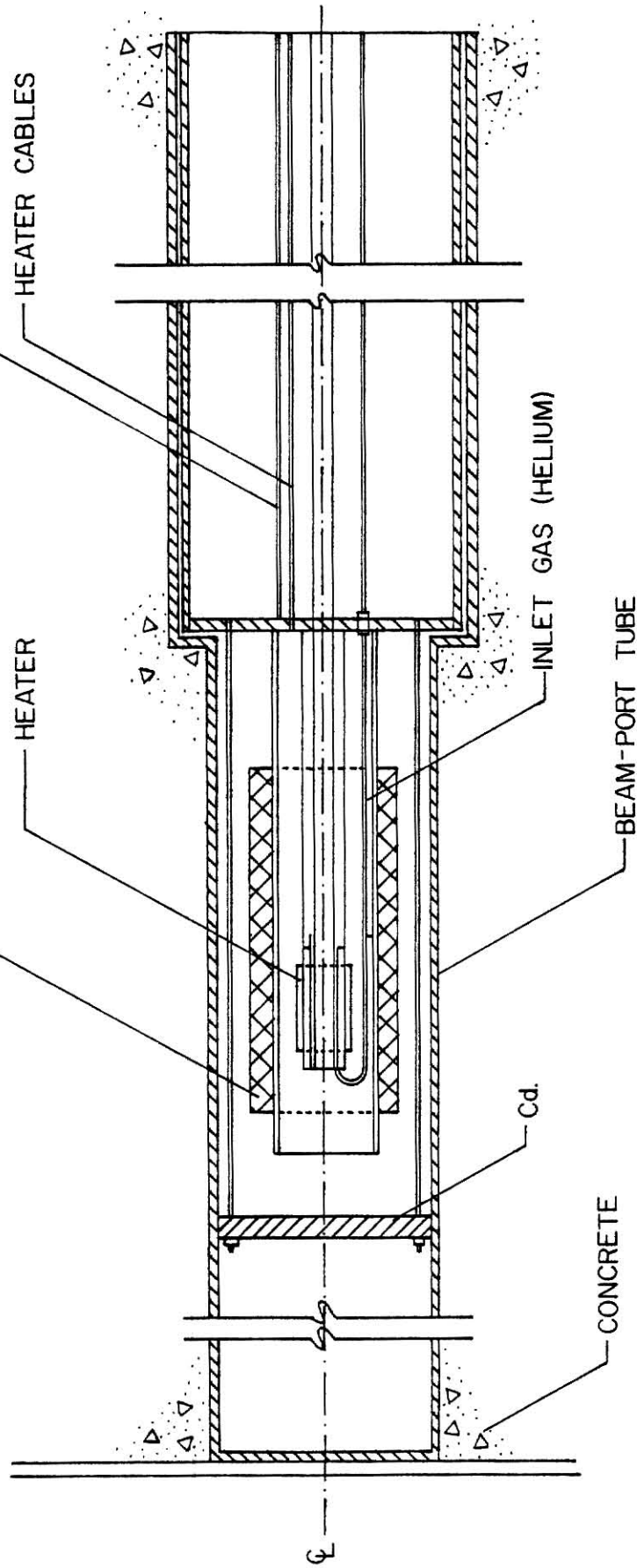

Fig. 2. DIAGRAM OF FAST NEUTRON IRRADIATOR AT ELEVATED TEMPERATURES POSITION RADIAL PIERCING BEAM-PORT

3.2.1. The Heater Structure

The heater structure was designed to accommodate a sample with maximum dimensions of 1 cm in diameter and 2.5 cm in length. The temperature inside the heating volume can be extended up to 900 K. The heater structure is composed of four substructures, these are the heater support, innertube, outer-tube, and an aluminum supporting disc. The diagram of the heater structure is shown in Fig. 3.

The heater is made from 1 mm Nichrome wire, wound on a porcelain holder. To minimize heat losses due to radiation, two layers of 2 mm asbestos sheet are wrapped around the heater (see Fig. 4). The heater is supported by a stainless steel tube, and the tube is attached to the aluminum supporting disc. Beside supporting the heater, the tube also acts as a heat conductor. The details are shown in Fig. 5. The reason for choosing stainless steel, instead of regular carbon steel, is to minimize the oxidation or corrosion on exposure to high temperatures. The purge gas flows through a copper pipe into the specimen chamber. The purge gas acts as a convective heat transfer medium and also to reduce the possibility of oxidation of the sample during irradiation at elevated temperature.

Surrounding the heater, two tubes are installed. These tubes are used to reduce the heat conduction and convection in the radial direction. The inner tube is made from carbon steel and covered with glass wool as an insulator. With the help of this insulator most of the heat is transferred by conduction. Outside the glass wool, an Iron-Constantan thermocouple is used to monitor the temperature. The inner tube is bolted

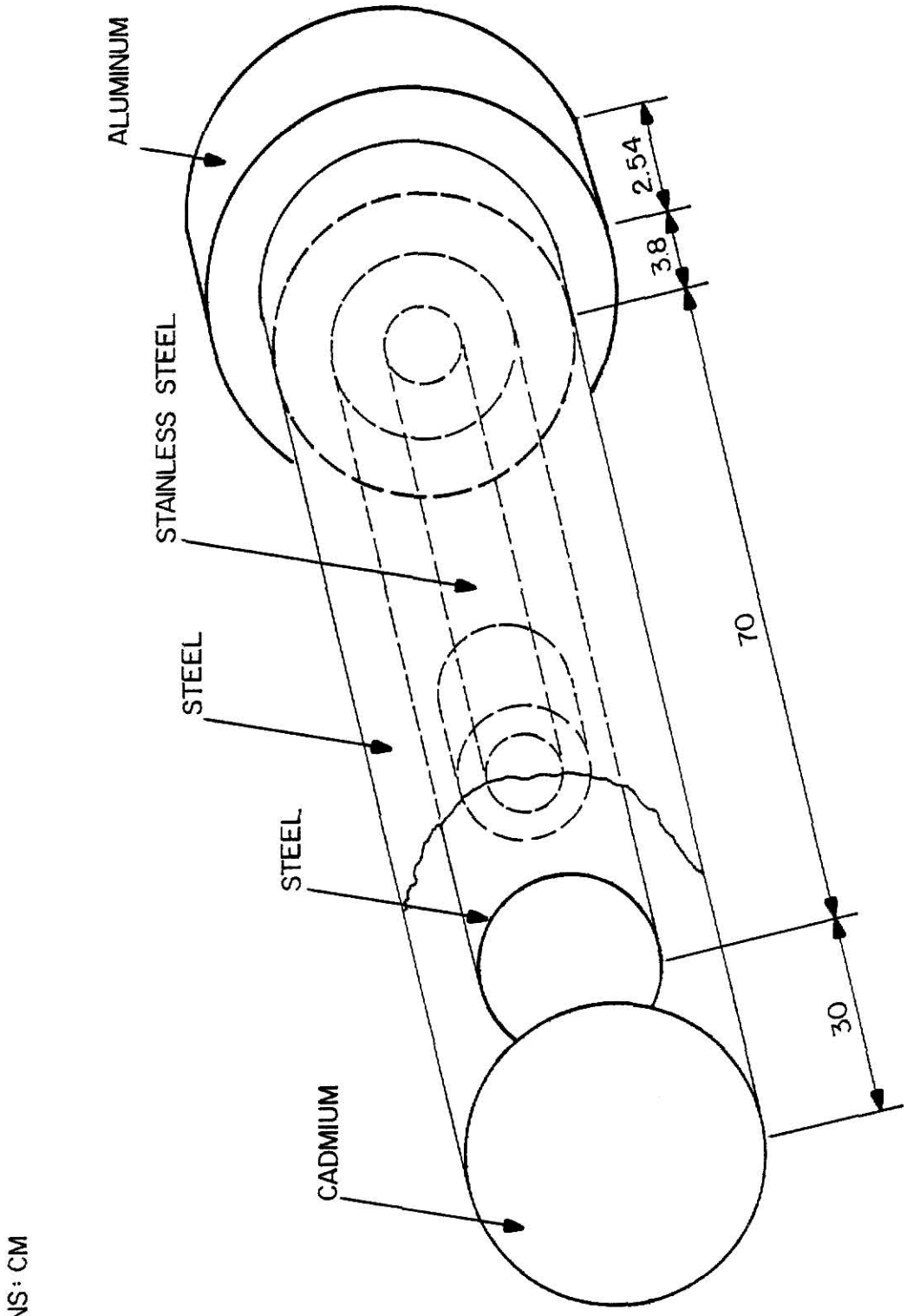

Fig. 3. The Diagram of the Heater Structure

DIMENSIONS : CM

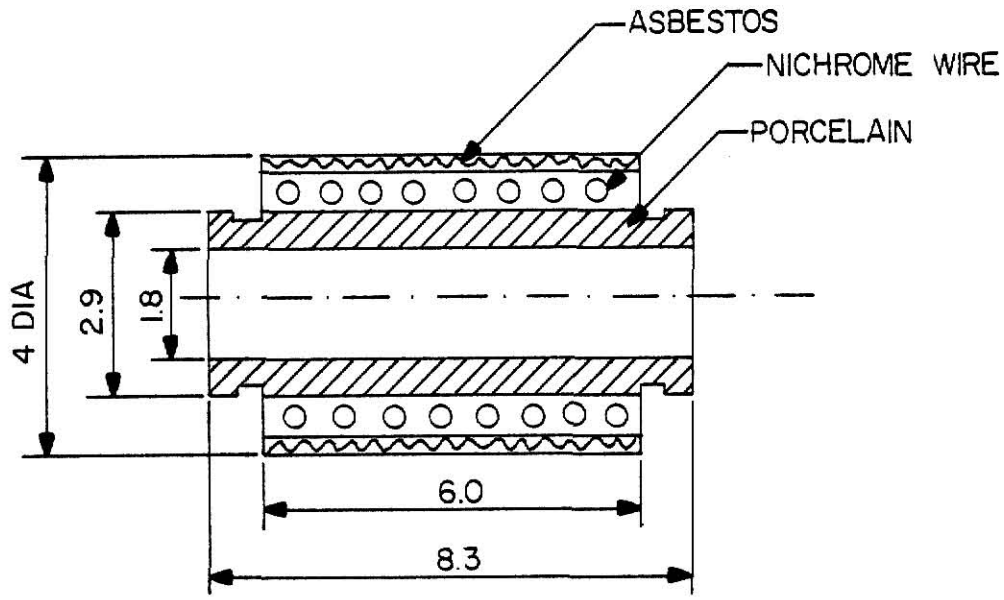

Fig. 4. Heating Element

DIMENSIONS : CM

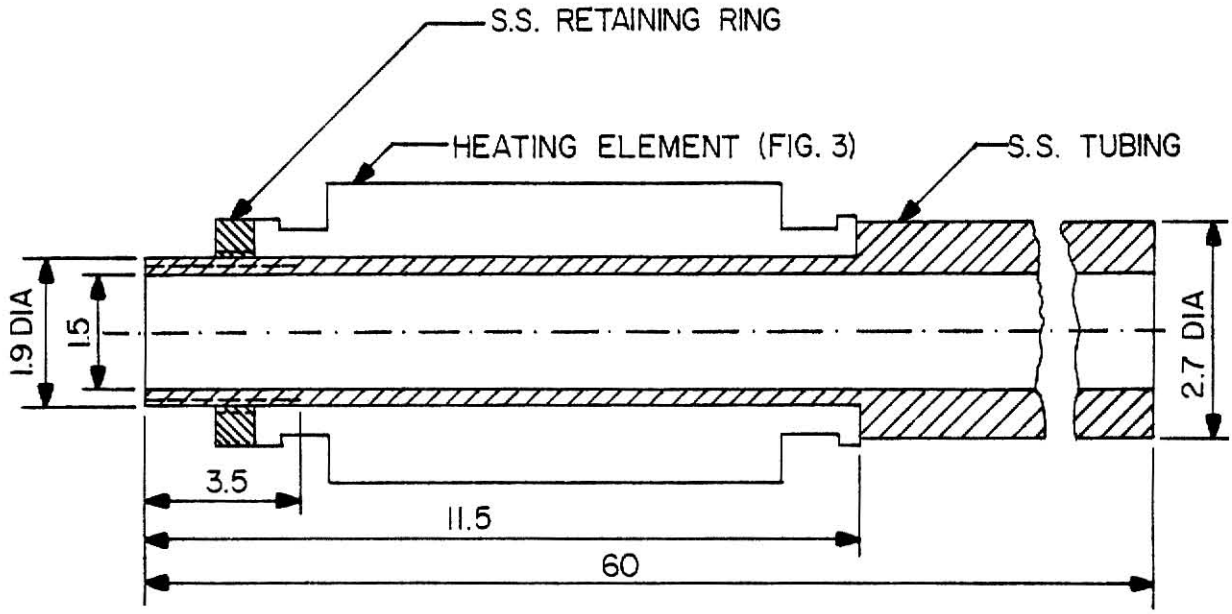

Fig. 5. Heating Element Support

to the aluminum supporting disc. Beside reducing the heat conduction in the radial direction, the outer tube is used also to attach the thermal neutron absorber, a 2 mm thick cadmium sheet. This cadmium sheet will absorb approximately 99.99% of the thermal neutrons. On the outside of the outer tube, another Iron-Constantan thermocouple is installed. The position is approximately above the heater. During operation, this thermocouple (T_3) is monitored continuously.

The supporting disc, which is made from aluminum, is used to join the heater structure and the beam plug structure. Figure 6 shows the shape and size of the disc. The disc also acts as a heat sink for the heat coming from the heater support, inner tube, and outer tube.

3.2.2. The Beamplug Structure

The main purpose of the beamplug is to attenuate both the neutrons and the gamma rays from the core. The neutrons from the core have a very wide spectrum, namely from thermal up to 20 MeV. A strong thermal neutron absorber will not attenuate the fast neutrons, thus a moderating material must be used to slow down the fast neutrons, then the thermal neutrons are absorbed with a strong thermal neutron absorber. The best choice for moderator is an element with low atomic number. Paraffin, in this case, is a very convenient choice, because it is easily mixed with borax, which is a strong thermal neutron absorber, and also paraffin is cheap.

The beamplug is made from a steel tube which fits the larger part of the beamport. On each end of the beamplug, 5 cm thick lead

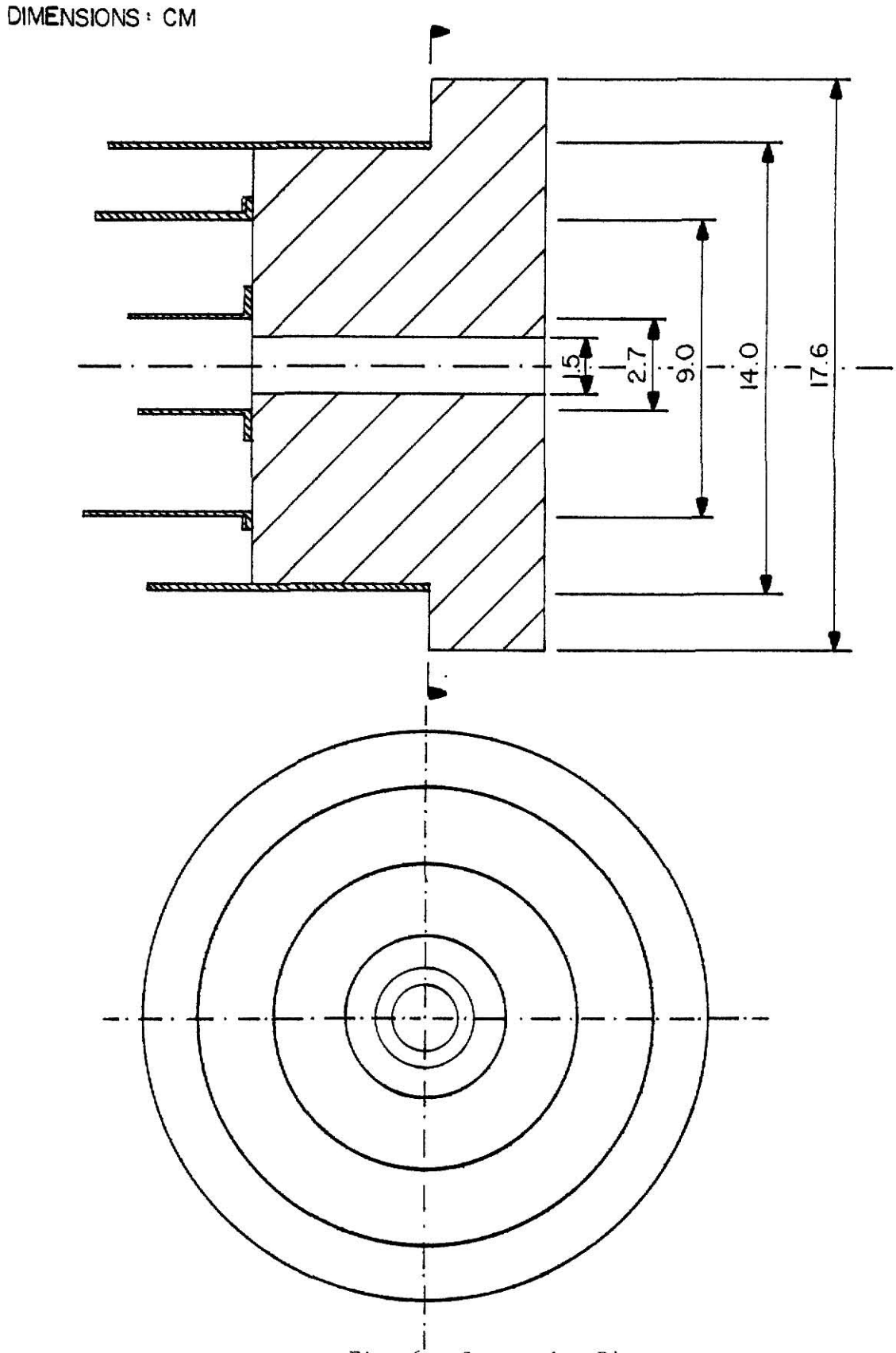

Fig. 6. Supporting Disc

disk are mounted. These lead discs attenuate the gamma ray flux. Between the lead discs, a borated paraffin is used to attenuate the neutrons. In the center of the beamplug, a square channel was installed. The channel cross section is 3.2 x 3.2 cm, and made from aluminum tube covered with cadmium. The channel is used to insert the specimen holder. Besides the square center channel, three other channels were made. These three channels serve for the placement of the thermocouple cables, the heater cables, and the purge gas plumbing. The three auxilliary channels were made from aluminum tubes.

3.2.3 Specimen Holder

The specimen holder structure can be divided into three parts. The front part, which is cylindrical, is located inside the heater support when the specimen holder is fully inserted into the irradiation chamber. The middle part is a square steel rod, and the rear part is a wooden rod, which has the same size as the middle part. The detailed drawing is shown in Fig. 7.

The front part is divided into two sections. The first section, which is directly exposed to a high temperature, is made from a stainless steel rod, and has a chamber for the placement of the sample. The chamber has an opening in the upper part. The size of the sample chamber is 1.3 cm in diameter and 2.5 cm long. The second section is made from a carbon steel rod. The first and second sections are screwed together. The overall size of the front part is 1.4 cm in diameter and 60 cm long, in which the first section is 20 cm in length.

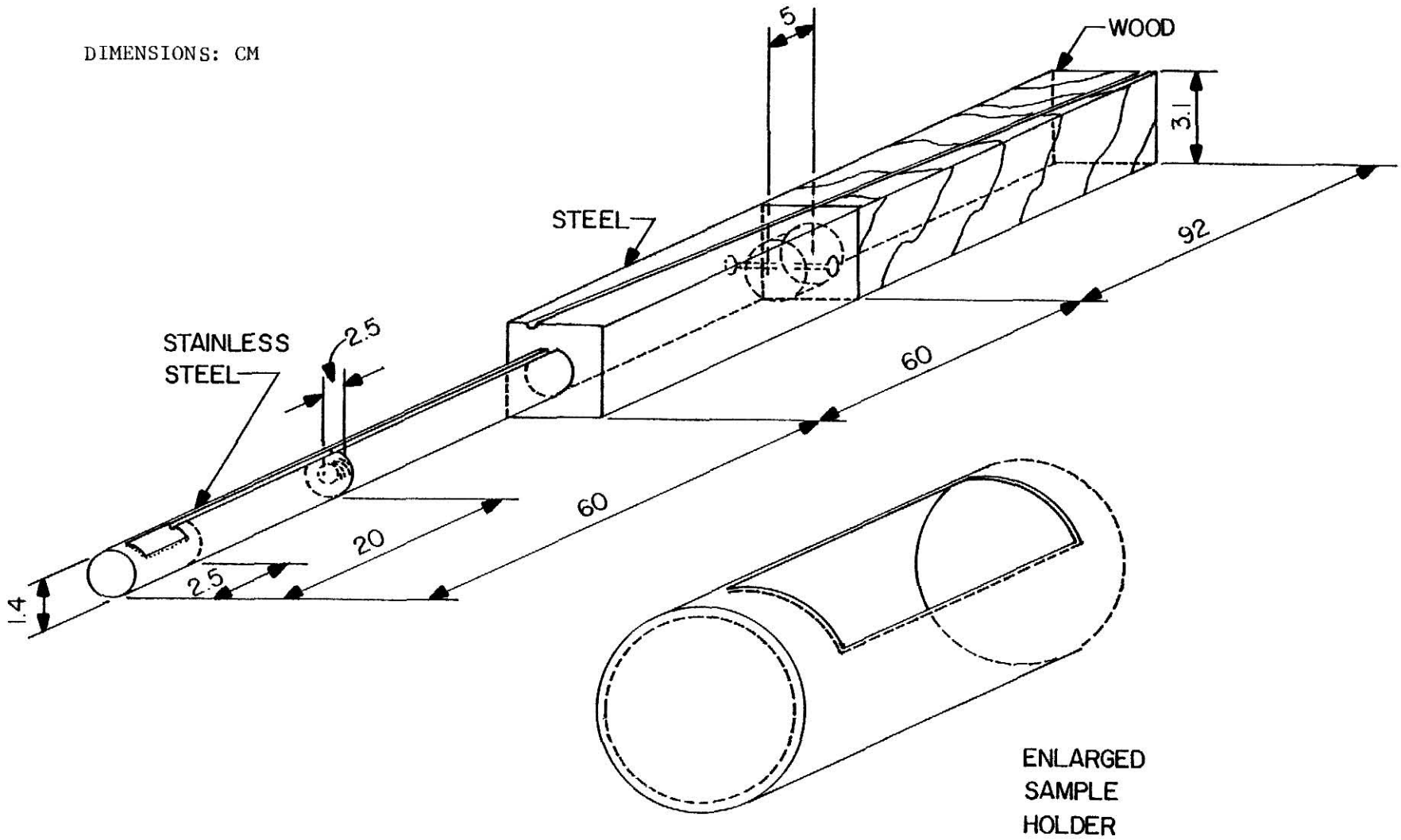

Fig. 7. Specimen Holder

In the upper side of this rod, a small channel was made for the placement of the Chromel-Alumel thermocouple, which is used to monitor the temperature inside the sample chamber.

The middle part of the specimen holder is a square carbon steel rod, with a cross section 3.1 x 3.1 cm. A small hole is provided to join the front part with the middle part, and strengthened with a steel pin. The middle part is 60 cm long, and serves to attenuate the gamma ray flux from the core.

The rear part, which is made from square wooden rod, has the same cross section as the middle part. The rear part is joined with the middle part in the same manner as the joint between the front and the middle part. The rear part serves to attenuate and moderate fast neutrons from the irradiation chamber. The length of the rear part is 92 cm.

On the upper side of the steel and wooden rod, a small channel was made also for the thermocouple cable. The channel was not made parallel to the side of the steel or wooden rod, but made a small angle to reduce the channeling of fast neutron.

3.2.4. Instrumentation

Two physical quantities, which must be monitored continuously during irradiation, are the purge gas flow rate and the temperature. The temperature is monitored continuously at three positions during irradiation. They are the chamber temperature, the surface of the inner tube, and the surface of the outer tube. Because the temperature

at the outer tube is directly related to the beamport liner temperature, the thermocouple in this position is connected to a separate voltmeter and recorded. A block diagram of the temperature measurement system is shown in Fig. 8.

To measure the power through the heater, a voltmeter and an ammeter are connected between the heater and the variable transformer. A six-ampere fuse is installed also to limit the current to the heater, so that the power will not exceed 200 watts, as approved by the Kansas State University Safeguard Committee (see Appendix II). To monitor the helium purge gas flow, which is set at 500 cm^3/min, a Fisher model 36-541-21 flowmeter is used.

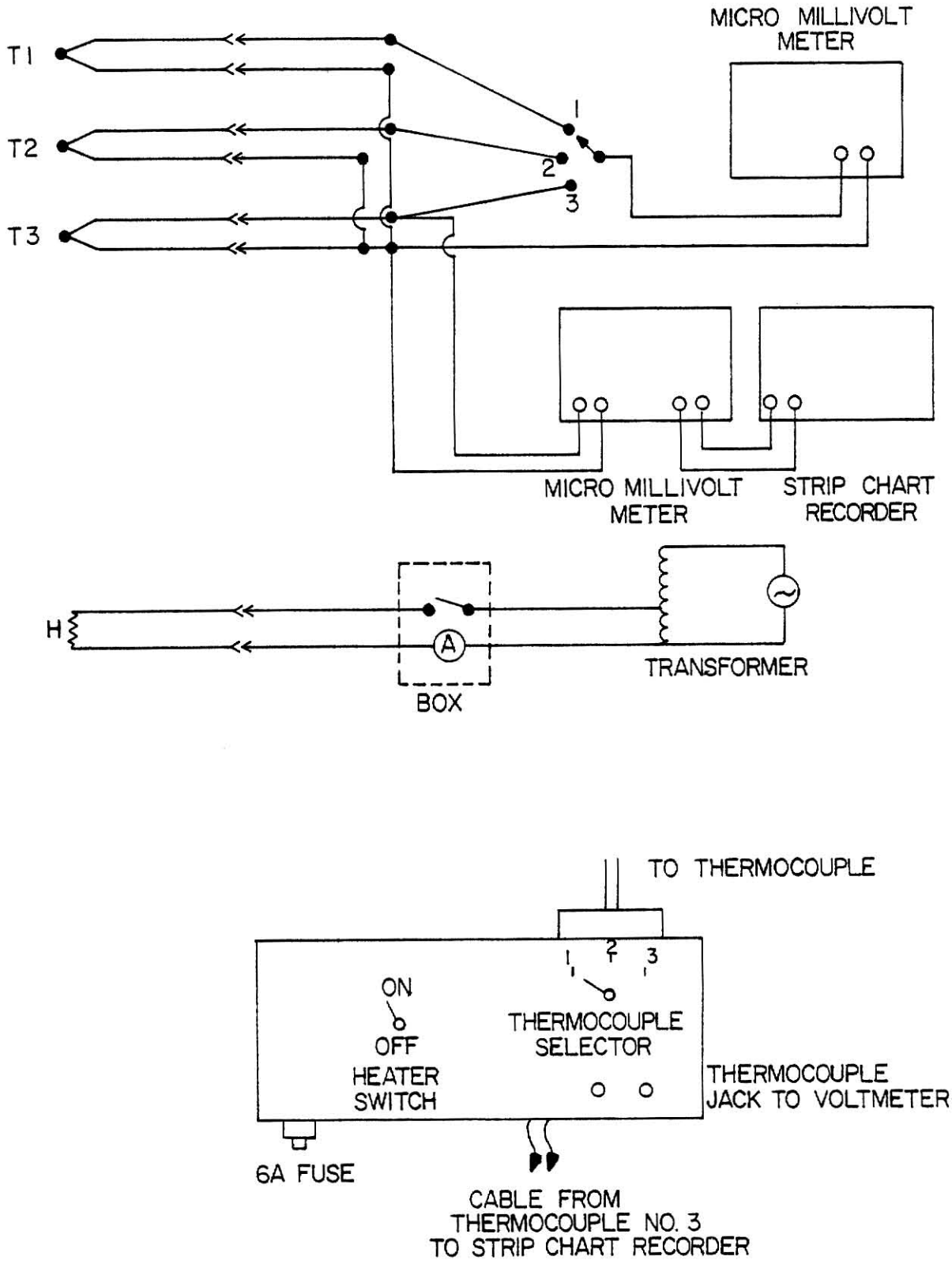

Fig. 8. Temperature Measurement System

4.0 SYSTEM CALIBRATION

Before and after the installation of the chamber into the beamport, four tests were performed to evaluate the chamber properties. The most important properties are the temperature distribution, radiation dose rate surrounding the beamport outlet, and the magnitude of the fast neutron flux in the irradiation chamber.

4.1 Temperature Distribution

In the introduction, it was explained that the temperature distribution in the area surrounding the heater is related to the safety of the reactor. If the concrete is exposed to a higher temperature than room temperature, the concrete will start to dehydrate, but up to certain temperature the mechanical integrity of the concrete will not change considerably. Water is bonded to the hardened concrete paste as water of crystallization, and there is also free water or moisture. When the concrete starts to dehydrate or some of the water in the hardened paste changes into free water, then the concrete will decrease in compression strength, flexure, tension, and density. Upon loss of water, concrete also tends to shrink; and if restrained, cracking may occur. According to David and Asce[9], the decrease in physical properties is quite small for a well-cured concrete up to 366 K. Even for a higher temperature, 548 K, the change in physical properties is ordinarily tolerable. Another concern with the release of the water from the concrete is the ability to attenuate the fast neutrons, because the neutron moderation in the concrete is mainly caused by the water molecules or more precisely the hydrogen atoms. Table 3 shows the data of the neutron mean free path as a function of temperature in the concrete[9].

Table 3. Fast neutron attenuation in an ordinary concrete shields.[9]

Temperature (^{o}C)	Density (g/cm^{3})	Mean Free Path (cm)
Room Temperature	2.35	12.06
100	2.29	12.80

In this design, it is required that the temperature of the concrete surrounding the chamber will not be higher than 50C. In order to meet this requirement, two tests were performed. The first test was a preliminary test in the beam plug storage hole. The storage hole has a similar structure and size as the inner section of the beamport, it is located in the south wall of the reactor bay. The hot spot on the outer tube of the irradiation chamber was determined before the chamber was inserted into the storage hole.

The temperature distribution measurement along the outer tube was conducted after the whole irradiation chamber was assembled. The purpose of this measurement was to locate the maximum temperature position or the hot spot position on the surface of the outer tube. It was found that the hot spot was approximately in the middle of the heater position. This is understandable, since purge gas only passes through the sample chamber and not between the heating chamber and the inner tube. The heat transfer is mostly due to radiation and free convection between the heater and inner tube or the inner tube to the outer tube.

An Iron-Constantan thermocouple was installed on the surface of the storage liner, before the irradiation chamber was inserted into the storage hole. The location of this thermocouple was right above the hot spot position. After the heater and the irradiation chamber was inserted into the beamplug storage hole, then the heater was turned on and increased step by step. At each increase the temperature at four locations, inside the heater chamber, outside surface of the inner tube, at the hot spot on the outer tube, and the storage liner, were monitored continously until the temperatures reached equilibrium. The maximum power applied to the heater was 200 watts and the maximum allowed current

was 6 amperes. The results from the preliminary test yielded the approximate correlation between the maximum temperature at the surface of the outer tube or the hot spot with the maximum temperature exposed to the beamport liner. The results of these measurements are shown in Table 4 and Fig. 9.

The result indicated that the liner temperature reached 50 C when the hot spot temperature was ≃ 130 C. If the hot spot temperature is kept below 130 C, it is unlikely that the concrete temperature will reach 50 C.

The final test was performed in the radial piercing beamport. The hot spot thermocouple was connected to a strip chart recorder in parallel with the monitoring volmeter. To minimize the possibility that the concrete temperature will not exceed 50 C, the maximum reading of the voltmeter must not be higher than 4 millivolt, which corresponds to a temperature of 96 C. If the hot spot temperature is 96 C the beamport liner temperature will be approximately 36 C, based on the results from the measurements in the storage hole. The first step was to energize the heater and wait until the equilibrium temperature was reached in the specimen chamber. Then the reactor was brought up to full power for two hours. If the hot spot temperature during the operation exceeded 96 C, the heater supply will be switched off and the purge gas flow is increased to maximum flow. The results are shown in Table 5 and Fig. 10.

The equilibrium temperature of the hot spot was reached in two hours after the power was applied to the heater, and the temperature was 83 C. At this temperature, the beamport liner temperature would be approximately 32 C. Thus the temperature of the concrete shield is less than the maximum permissible temperature.

THIS BOOK CONTAINS NUMEROUS PAGES WITH DIAGRAMS THAT ARE CROOKED COMPARED TO THE REST OF THE INFORMATION ON THE PAGE.

THIS IS AS RECEIVED FROM CUSTOMER.

Table 4. Temperature vs. Heating time. Current: 6 amperes; Voltage: 30 volts; Coolant: He (500 ml/min); Room temperature: 21°C.

Time of Heating (Minutes)	Temperature Inside the Heater (°C)	Temperature of the Hotspot	Temperature at the Liner
15	529	37	22
30	647	67	28
45	659	94	35
60	670	110	40
75	670	120	46
90	670	125	48
105	670	129	50
120	670	131	52
135	670	133	54

Fig. 9. Temperature vs Heating Time in the Beamport Storage Hole

Voltage: 30 V

Current: 6 A

Coolant: Helium (500 ml/min)

Room Temperature: 21 °C

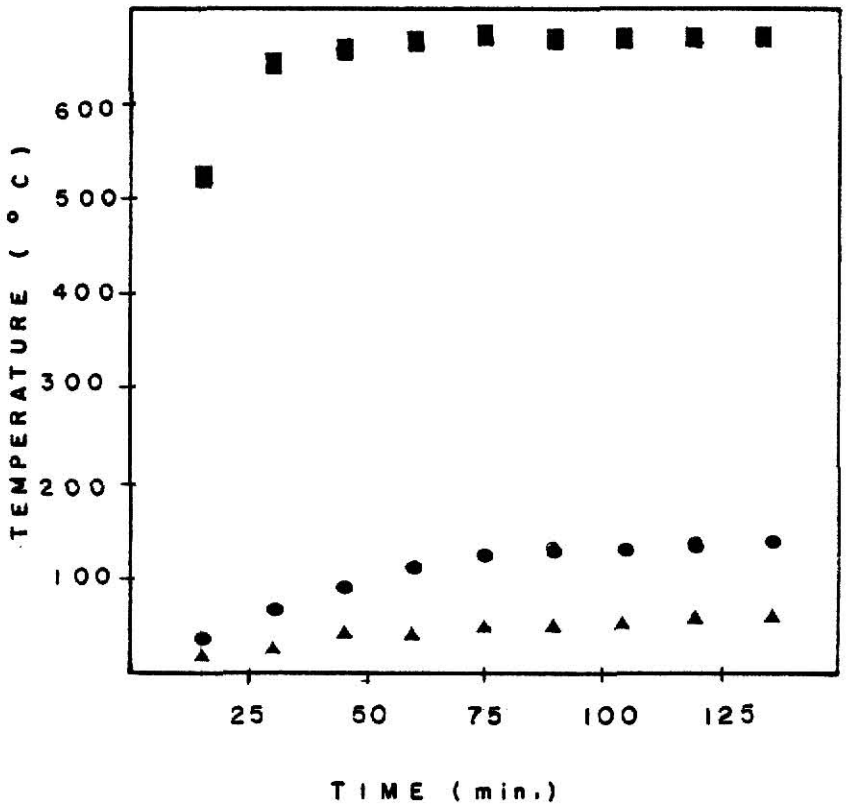

■ Temperature inside specimen chamber

● Temperature at the hot spot

▲ Temperature at the liner

Table 5. Temperature irradiation chamber vs. time inside the radial piercing beamport. Current: 5.7 amperes; voltage: 30 volts; coolant: He (500 ml/min); room temperature: 18°C; reactor power: 225 kW.

Time (min.)	Specimen Chamber Temperature (°C)	Inner Tube Temperature (°C)	Outer Tube Temperature (°C)
10	451	64	21
20	548	119	31
30	597	153	53
40	601	73	68
50	601	182	76
60	601	182	78
70	601	182	80
80	601	182	80
90	601	182	82
100	601	182	82
110	601	182	83
120	601	182	83
130	601	182	83
140	601	182	83
150	601	182	83
160	601	182	83

Fig. 10. Temperature vs Heating Time in The Radial Piercing Beamport

Voltage: 30 V

Current: 5.7 A

Coolant: Helium (500 ml/min)

Reactor Power: 225 kW

Room Temperature: 18 °C

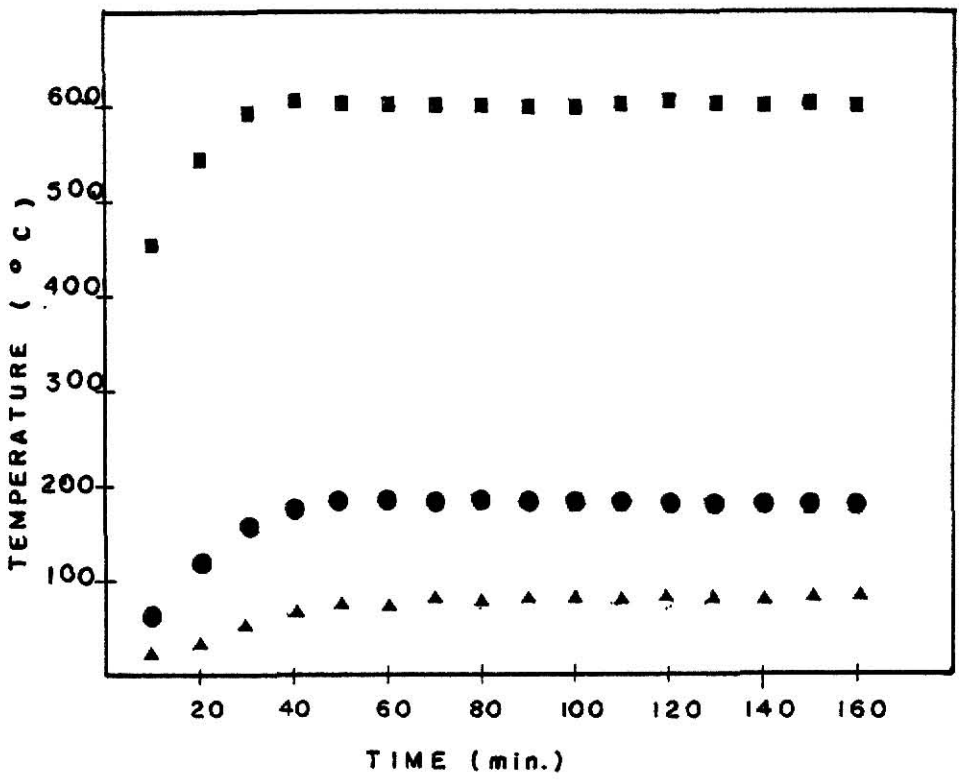

■ Temperature inside specimen chamber

● Temperature outside inner tube

▲ Temperature on the hotspot

4.2. Radiation Hazard

A radiation hazard test is necessary, mainly because regulations require such a test for a new installation of equipment in the reactor. Secondly, because the temperature may not exceed the permissible value and also the purge gas must be kept at a constant flow rate, hence, one must work at the instrument location, which is approximately 2.5 m from the beamport. According to 10 CFR20, a working area (radiation area) may not exceed a dose rate of 5 mrem/hr. or 100 mrem in any 5 consecutive days.

Two types of radiation monitoring instruments were used for this test, these are one neutron survey meter (Texas Instruments Model 9146) and one gamma survey meter (Eberline Model 942). The reactor was brought into operation gradually, started from lowest power, i.e., milliwatts, to full power. At each power increase the dose rate surrounding the beamport were measured.

The radiation hazard survey was conducted, when the irradiation chamber was installed into the radial piercing beamport. Four areas surrounding the beamport were surveyed using both gamma and neutron survey meters. The locations of the measurements are shown in Fig. 11. The results, as the power was increased, are shown in Table 6.

A beam catcher made from borated parafin was placed in front of the beamport. It provides extra neutron shielding. The dose rate in front of the beam port was relatively higher in a narrow region. This is due to the fact that the wood in the specimen holder is a less efficient neutron absorption compared to the borated parafin. With the addition of beam catcher in front of the narrow beam of neutrons, the dose rate is

TABLE 6
RESULT OF RADIATION HAZARD SURVEY
SURROUNDING THE RADIAL PIERCING BEAMPORT

POWER (WATT)	LOCATION 1 (mR/Hr)	2 (mR/Hr)	3 (mrem/Hr)	4 (mR/Hr)
0.01	0	0	0.02	0
1	0	0	0.02	0
100	0	0	0.02	0
10^4	0	0	1.5	0
10^5	0	2	13	0
2.25×10^5	0	100	28	0
2.25×10^5 (with beam catcher)	0	40	1	0

Note: Location 1 Detector G.M.
2 Detector G.M.
3 Detector neutron
4 Detector G.M.

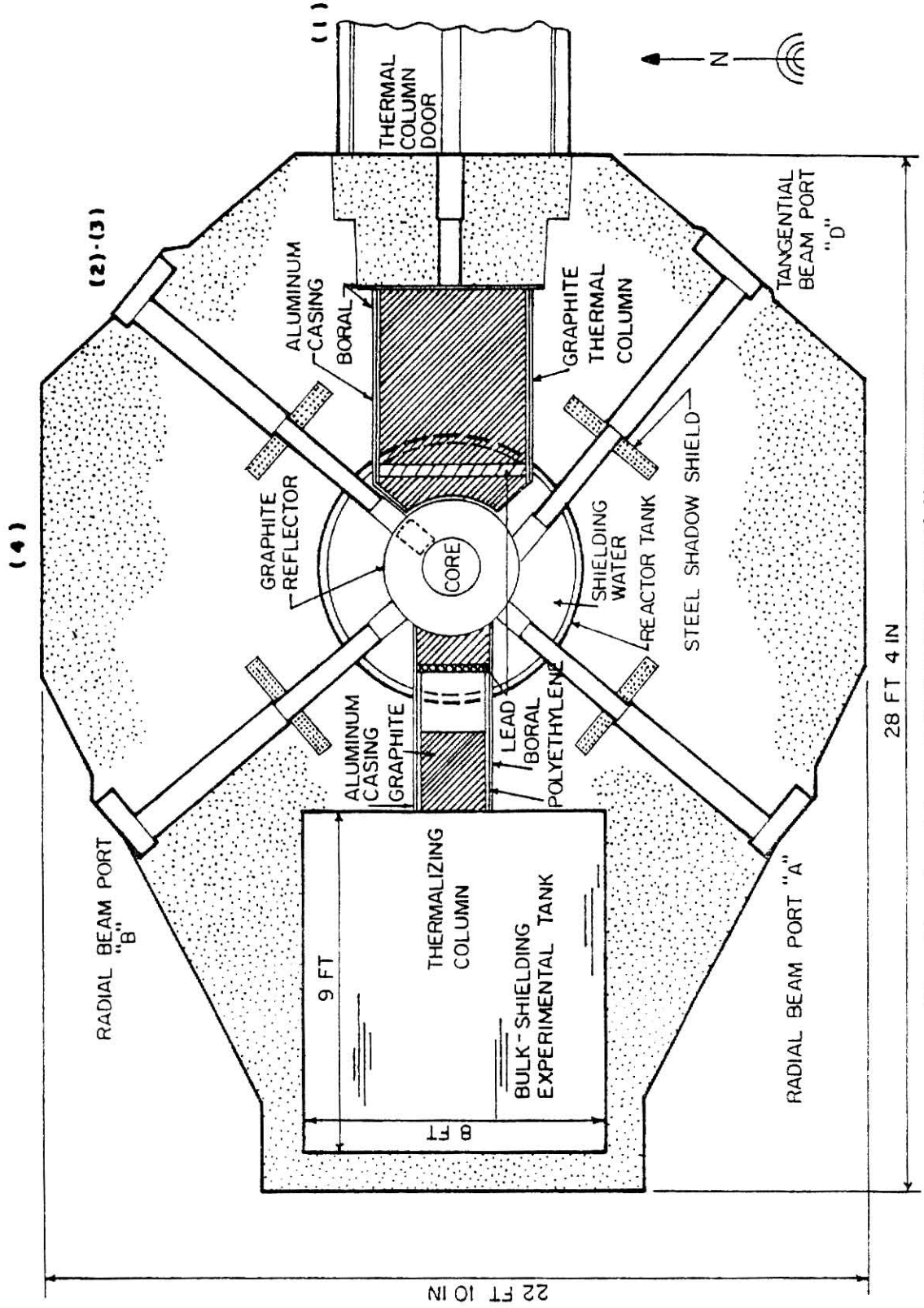

Fig. 11. Location of Radiation Hazard Measurement

reduced down to 1 mrem/hr. In the area beside the beamport, the dose rate is less than 2 mrem/hr. The area is safe enough for an individual to monitor the instrumentation while the reactor operates at full power.

4.3 Flux Measurement

4.3.1. Neutron Spectrum in the Radial Piercing Beamport

The fast neutron energy spectrum in the radial piercing beamport is similar to the energy spectrum at the core surface, because approximately 2 cm of aluminum is the only material which is between these two positions. The total cross section for aluminum with neutron energy at 1 MeV is only 3 barns and decreases with increasing neutron energy. The major attenuation in the flux is due to the geometrical attenuation. The experimental data for the fast neutron energy spectrum at the radial piercing beamport or at the ring-F of the core are not available. The complete neutron energy spectrum which is available has been calculated by West[8]. The calculated neutron flux using multigroup diffusion theory is published in GA-4361.

In Fig. 12, the calculated fast spectrum of West at ring-F is compared with the empirical fission spectrum for U-235 by Cranberg and Frye. These two spectra are averaged for three energy intervals, which correspond to the effective energy interval of the detectors used in these measurements, and normalized to the highest energy interval. The empirical formula for the fission spectrum of U-235 proposed by Cranberg and Frye[26] is

$$\chi(E) = 0.453 \exp(-1.036E) \sinh(\sqrt{2.29E}) \qquad (4.3.1)$$

where E is the energy in MeV.

4.3.2. The Measurement of the Thermal Neutron Flux[13]

The thermal neutron flux can be measured in a number of ways, such as foil activation, photographic emulsion, thermoluminesence detector

Fig. 12. Comparison of Neutron Spectrum at Ring -F

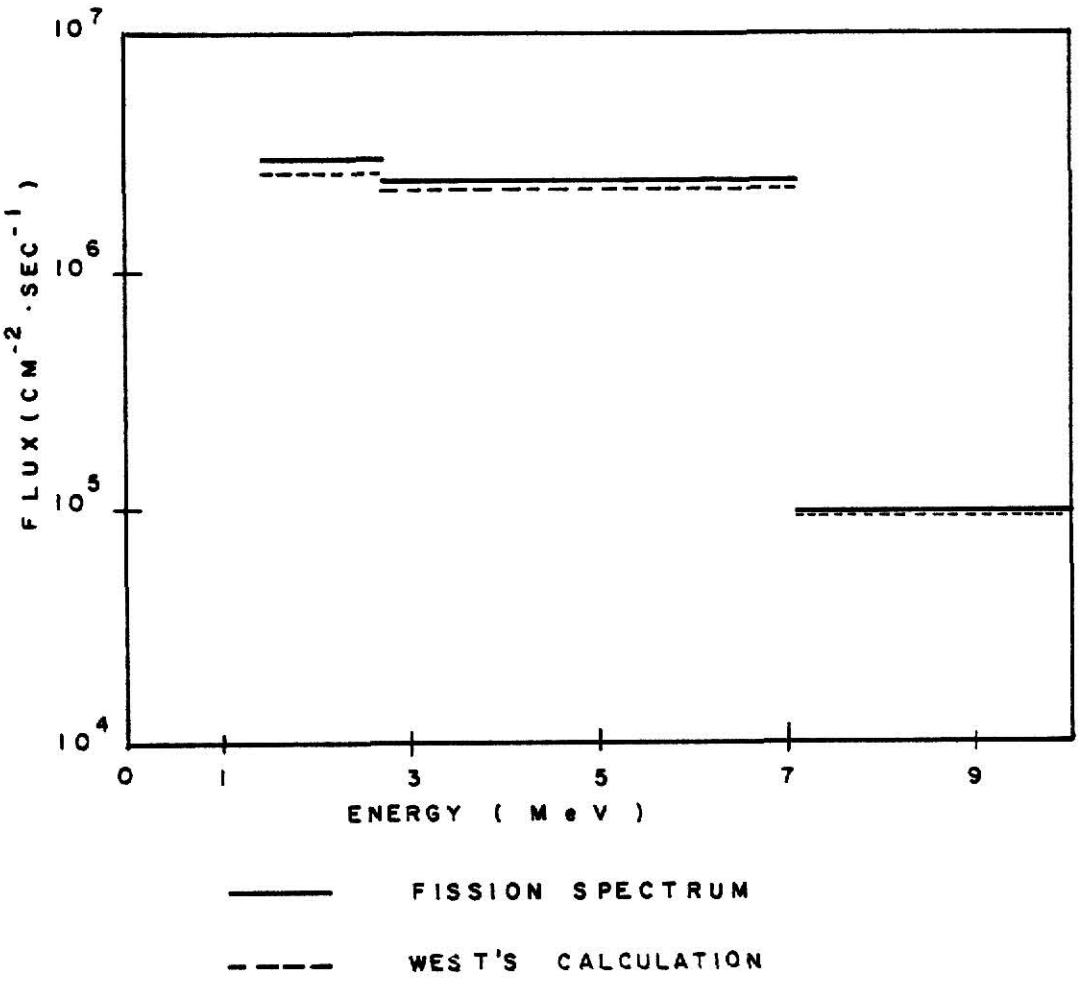

and others. Among these methods, the foil activation is the most popular, because this method gives accurate results with a relatively easy procedure. With the appropriate type of detector and procedure, it can cover the range from a low neutron flux ($\sim 10^{7}$ n/cm^{2}· s) to a high neutron flux ($\sim 10^{15}$ n/cm^{2}·s). The disadvantage of foil activation detection is that the result can not be obtained instantaneously, because the activation product must be measured with another radiation detector to determine the neutron flux. Another disadvantage of this method is that the result is an average value of the flux during irradiation, hence this method can not be used to measure a time dependent neutron flux.

For the measurement of the thermal neutron flux inside the beamport, gold foil was chosen. The main reason of choosing gold foil as the activation detector is due to the fact that the activation cross section is relatively large, i.e. $\sigma_{act.}$ = 98.5 barn[12], and the activation product is a β-γ emitter, with half life of 2.7 days and γ-energy of 0.41 MeV[12, 14]. Before the installation of the irradiation chamber, the flux at eight positions radially distributed inside the beamport, were measured. The foils were attached to the front of a plastic disc, and kept in place using scotch-tape. Fig. 13 shows the position of the foils in the beamport.

To measure the activation product, a Ge(Li) detector was employed. The detector efficiency was determined using a standard source, that contains Co-60, Cs-137, Sn-113, Mn-54, Co-57, and Cd-109. These radioisotopes cover the energy range from 0.088 MeV(Cd-109) to 1.33MeV(Co-60).

If an activation foil with atomic density N_d(atoms/cm^{3}) and $\sigma_a(E)$(cm^{-2}) is the microscopic activation cross section at energy, E, $\phi(E)dE$ (n/cm^{2}·sec) is the neutron flux at that energy. The reaction

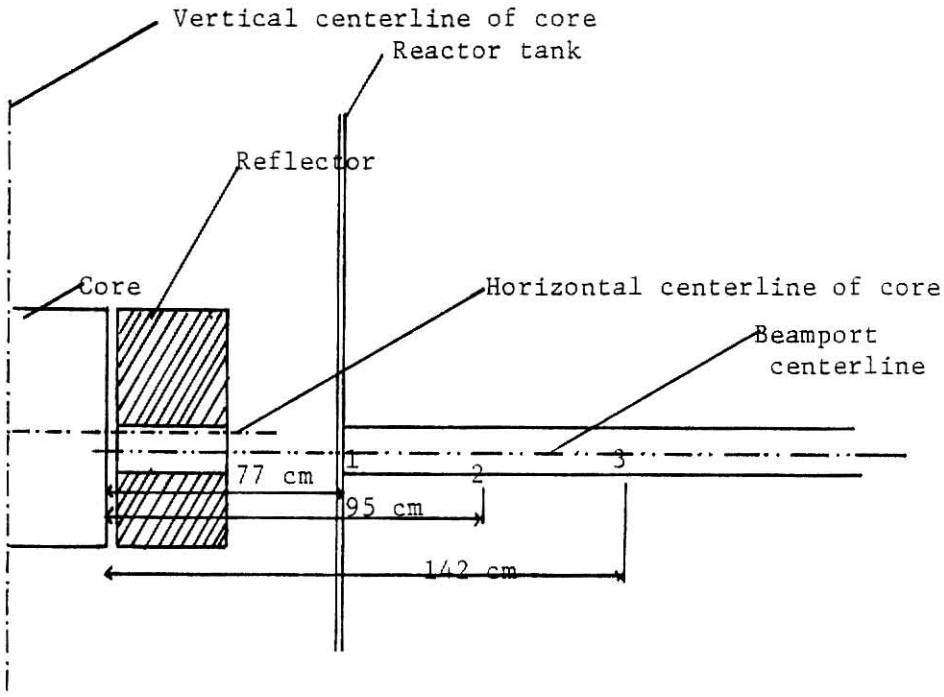

Figure 13.

1. Location of first thermal neutron measurement
2. Location of Cadmium absorber
3. Location of sample chamber

rate per unit volume in the detector can be expressed as

$$R(E)dE = N_d\ \sigma_a(E)\ \phi(E)dE. \qquad (4.3.2.)$$

The total reaction rate for energy interval 0 to ∞ is

$$R=\int_0^\infty R(E)dE = N_d\int_0^\infty \sigma_a(E)\ \phi(E)dE. \qquad (4.3.3)$$

The neutron flux in the reactor can be considered to be composed of two groups, a thermal group and fast group. The thermal group is defined for those neutrons whose energy is between 0 to 0.2 eV, and the fast group is defined for energy above 0.2 eV. Using this approximation, the total reaction rate is

$$R = N_d\ \bar{\sigma}\ \phi_{th} + N_d\int_{E_{TC}}^{E_{max}} \sigma_a(E)\phi d(E) \qquad , \qquad (4.3.4)$$

where

E_{TC} = thermal cutoff energy (∿0.2eV),

E_{max} = maximum energy of neutron (∿20MeV),

ϕ_{th} = thermal neutron flux,

$\bar{\sigma} = (\frac{\pi}{4})^{\frac{1}{2}}\ \sigma_a(E_T)$,

and

E_T = most probable neutron energy at 298 K.

To evaluate the reaction for fast neutron group we introduce E_{CC}, which is the effective Cadmium cut off energy, 0.4eV, and rewrite the reaction rate for the fast neutron group as

$$R_{fast} = N_d \int_{E_{TC}}^{E_{CC}} \sigma_a(E)\phi(E)dE + N_d \int_{E_{CC}}^{E_{max}} \sigma_a(E)\phi(E)dE. \qquad (4.3.5)$$

The total reaction rate becomes

$$R = N_d \left(\bar{\sigma}\, \phi_{th} + \int_{E_{TC}}^{E_{CC}} \sigma_a(E)\phi(E)dE + \int_{E_{CC}}^{E_{max}} \sigma_a(E)\phi(E)dE \right). \qquad (4.3.6)$$

To measure the thermal neutron flux, the measurement has to be done in two steps. The first step is by irradiating the bare foil, which gives the activation due to both thermal and fast neutrons. The second step is the radiation of the cadmium covered foil, where the activation is mainly due to the neutrons with energies above E_{CC}, or mathematically,

$$R_{Cd} = \int_{E_{CC}}^{E_{max}} \sigma_a(E)\phi(E)dE \quad . \qquad (4.3.7)$$

The integral expression is called the "resonance integral" of the detector, a quantity which has been measured for a large number of materials. For gold foil the value of the resonance integral is $\simeq$ 1558 barn[20]. By subtracting the reaction rate measured by the cadmium covered foil from the reaction rate measured by the bare foil, the reaction rate, caused by the thermal neutron flux and a small part of the fast neutron flux is given by

$$R_{th} = R_{bare} - R_{cd} = N_d \left(\bar{\sigma}\phi_{th} + \int_{E_{TC}}^{E_{CC}} \sigma_a(E)\phi(E)dE \right) . \qquad (4.3.8)$$

In practice, the value of the second term, which is called the activation due to subcadmium neutrons, is much smaller compared to the thermal neutrons, and is neglected. Since R_{bare} and R_{cd} are determined experimentally, then

ϕ_{th} can be determined. A more complete derivation is given in Appendix II.

The thermal neutron flux measurement was performed in three positions (see Fig. 13). The first position was at the inner end of beamport, which was adjacent of the reactor tank. The second measurement was at a distance 18.3 cm from the first measurement, which is approximately at the outer tube. The third measurement was at the specimen chamber. For the first and the second measurement, there were eight positions for each measurement as shown in Fig. 14.

During the evaluation of the data, three corrections were made. The first correction was for self-shielding. Self-shielding is defined by the ratio of the average flux through the foil volume to the average flux over the foil surface. The second correction is for flux perturbation, which is defined as the ratio of the activation of a foil in a perturbed flux to that which would result in an unperturbed flux. Because the foil was thin (0.07 mm thick), the corrections due to self-shielding and flux perturbation were small (less than 1%). A further discussion of these corrections is in Appendix II. The third correction was due to the self-absorption by the sample during counting. If μ is the absorption coefficient of the sample for the gamma ray emitted by the sample itself, then the self-absorption coefficient, f(x) is expressed by[28]

$$f(x) = \frac{(1-e^{-\mu x})}{\mu x} \qquad (4.3.9)$$

The results of the first measurement are shown in Table 7. From these results, a vertical and horizontal distribution of thermal neutrons in the beamport can be drawn. These are shown in Figs. 15 and 16. From these figures, it can be seen that the thermal neutron distribution is not

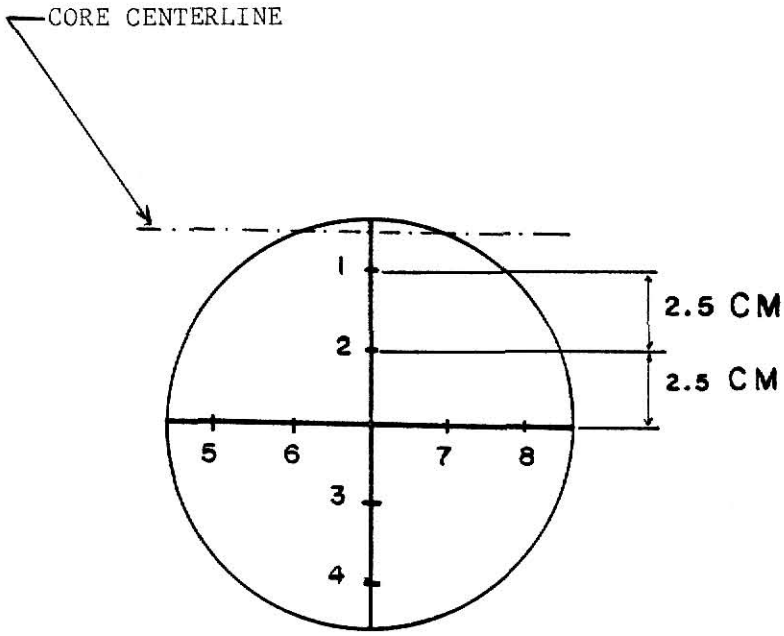

Fig. 14. Location of Flux Measurement Before the Installation of the Irradiation Chamber

Table 7. Thermal neutron flux at the inner end of beamport.

Position	Thermal Flux at 250 kW $\{cm^{-2}\ sec^{-1}\}$
1	$2.096 \times 10^{11} \pm 6.4 \times 10^{8}$
2	$2.218 \times 10^{11} \pm 6.5 \times 10^{8}$
3	$2.322 \times 10^{11} \pm 6.7 \times 10^{8}$
4	$2.495 \times 10^{11} \pm 6.8 \times 10^{8}$
5	$2.271 \times 10^{11} \pm 6.5 \times 10^{8}$
6	$2.355 \times 10^{11} \pm 6.7 \times 10^{8}$
7	$2.284 \times 10^{11} \pm 6.6 \times 10^{8}$
8	$2.495 \times 10^{11} \pm 6.7 \times 10^{8}$

symmetrical about the radial center of the beamport. The main reason is the effect of shim control rod. Fig. 19 shows the position of the shim control rod with respect to the position of the radial piercing beam port. During this measurement the shim rod was not fully withdrawn from the core, as a result the shim control rod depressed the thermal neutron flux. From Fig. 15, if the shim rod is fully withdrawn, the flux at positions 1 and 2 must be higher than positions 3 and 4, because they are closer to the core center (see Fig. 14). Also the flux at positions 6 and 7 should be higher than positions 5 and 8, which is not so.

On the second measurement, the shim rod was fully withdrawn from the core. It is shown in Figs. 16 and 17 and tabulated in Table 8. In this measurement the distribution is slightly better than the first measurement.

The vertical distrubution shows that the flux decreases as the distance from the core center increases. The difference between the uppermost and lowest position is only about 2.3%, while from the first measurement it is about 16%. From the horizontal distribution, the depression due to the effect of shim rods is less for the second measurement than from the first one.

The thermal neutron flux at the specimen chamber at 1 kW of power is $1.754 \times 10^{6} \pm 1.65 \times 10^{5}$ (cm^{-2} sec^{-1}), or $4.385 \times 10^{8} \pm 4.13 \times 10^{7}$ (cm^{-2} sec^{-1}) at 250 kW. With a 2 mm cadmium absorber, the calculated attenuation is 99.99%. The experimental results indicate that the attenuation is only $\simeq$ 99%. The reason is that the diameter of the cadmium sheet is less than the diameter of the liner of the inner beamport. As a consequence there is a gap between the cadmium and the beamport liner. Some of the neutrons pass through the gap and are scattered by the beamport wall into the detector.

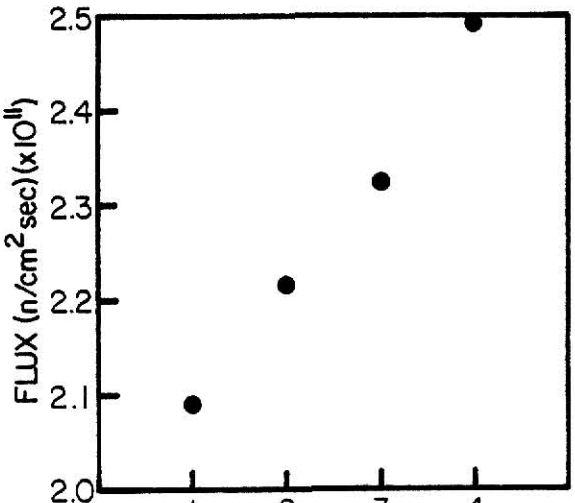

FIG. 15

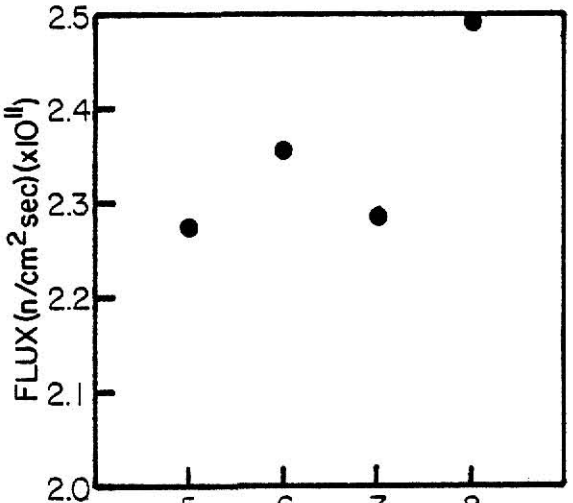

FIG. 16

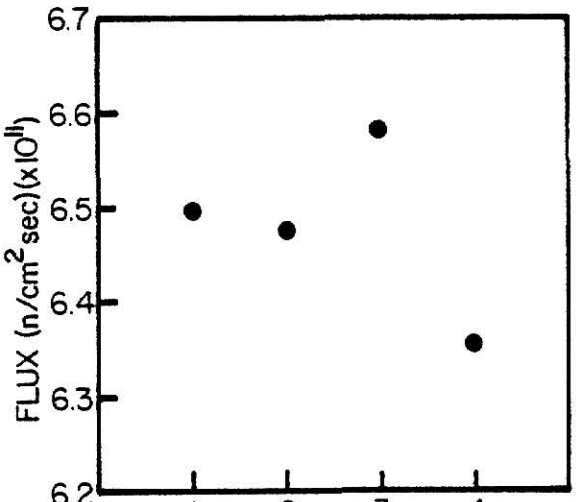

FIG. 17

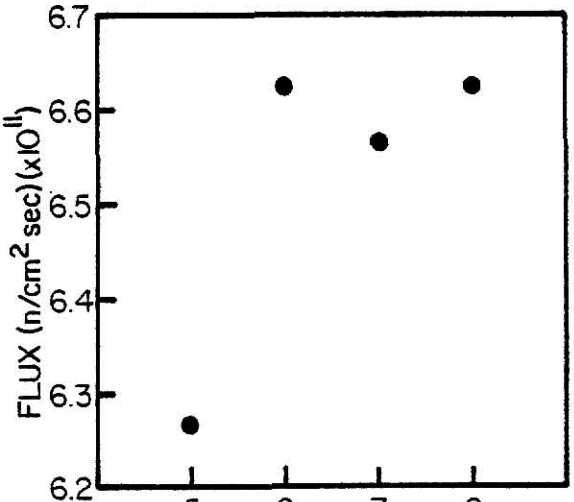

FIG. 18

ILLEGIBLE DOCUMENT

THE FOLLOWING DOCUMENT(S) IS OF POOR LEGIBILITY IN THE ORIGINAL

THIS IS THE BEST COPY AVAILABLE

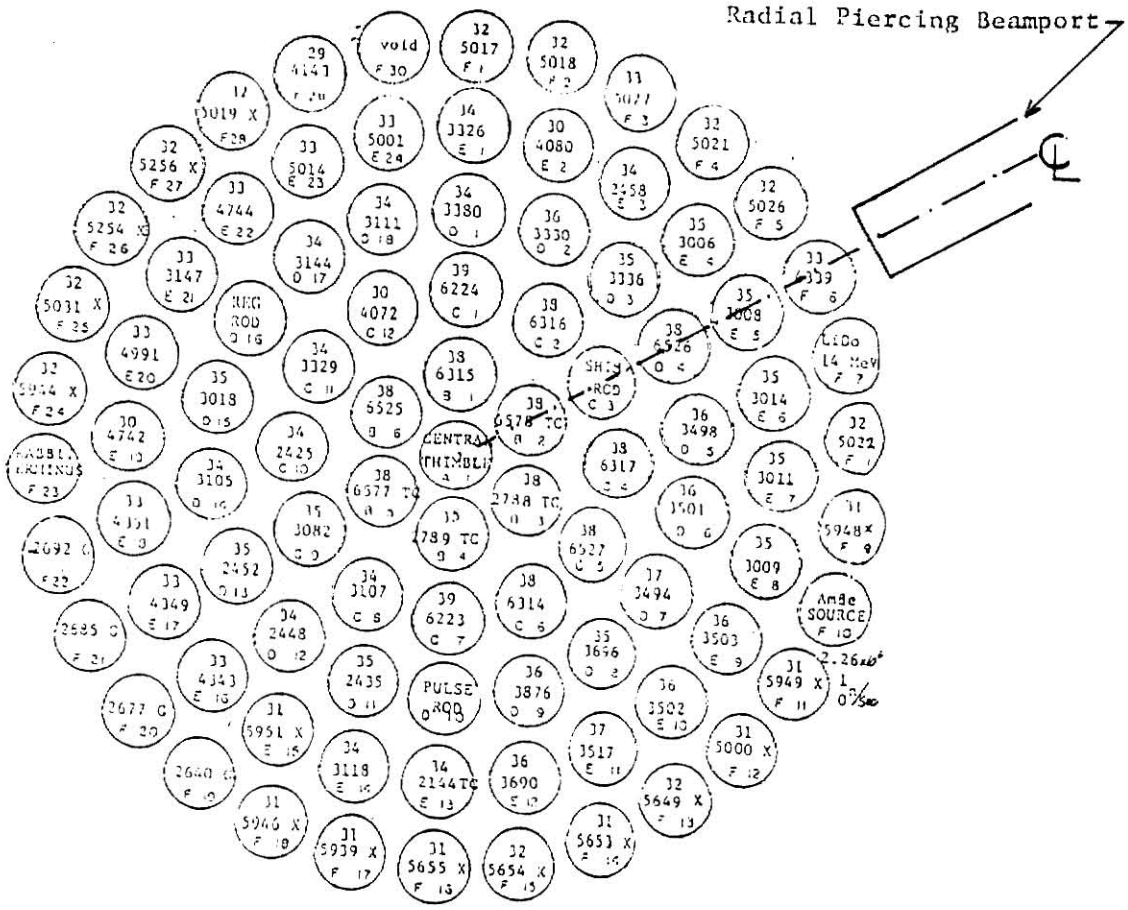

Figure 19. Position of Shim Rod with Respect to Beamport.

Table 8. Thermal neutron flux at end of outer tube.

Position	Thermal Neutron Flux (cm^{-2} sec^{-1}) 250 kW
1	$6.499 \times 10^{10} \pm 3.5 \times 10^{8}$
2	$6.473 \times 10^{10} \pm 3.5 \times 10^{8}$
3	$6.558 \times 10^{10} \pm 3.6 \times 10^{8}$
4	$6.555 \times 10^{10} \pm 3.6 \times 10^{8}$
5	$6.266 \times 10^{10} \pm 3.4 \times 10^{8}$
6	$6.626 \times 10^{10} \pm 3.6 \times 10^{8}$
7	$6.564 \times 10^{10} \pm 3.6 \times 10^{8}$
8	$6.627 \times 10^{10} \pm 3.6 \times 10^{8}$

4.3.3 The Measurement of the Fast Neutron Flux

Fast neutron flux and energy spectrum measurements can be done in several ways, i.e., proton recoils, photographic emulsion, time of flight and threshold reaction. The use of threshold detection has been developed intensively in the last 20 years. Six elements, namely Cu, Al, Fe, Ni, S and Ti, are commonly used as detectors[15]. The basic principle is that there is a nuclear reaction which becomes possible only if the neutron energy is above a certain value, the threshold energy. There are a number of reactions which can be used for the detection, e.g., (n,2n), (n,p), (n,n') and (n,α) reactions. Below the threshold energy, the reaction cannot occur. Hughes[16] introduced this method of evaluation in 1952. The method is based on the assumption that the cross section is a step function above the effective threshold energy. The magnitude of the cross section is taken from the maximum value of the actual cross section, and then using this value, the effective threshold energy, (E_{th}), can be evaluated using the relation

$$\int_0^\infty dE\ \sigma(E)\ \phi(E) = \sigma_{max} \int_{E_{th}}^\infty \phi(E)\ dE\ , \qquad (4.3.10)$$

where $\phi(E)$ = fission spectrum,

$\sigma(E)$ = energy dependent activation cross-section.

There are other methods used in evaluating the results. (For a comprehensive discussion, see Ref. 12. All references in this thesis are from that discussion.) Fisher, Dietrich, and Uthe[12] used a multigroup method to evaluate the result. Hartman[12] used a series of auxiliary functions in the evaluation. A semi-empirical method was developed by Grundl and Usner[12].

They recommend that one use the cross section and the threshold energy in such a way, that if the spectrum changes slightly from the fission neutron spectrum, these values change as little as possible. Uthe[12] recommends the use of a polynomial in energy for the spectrum.

In this measurement, the method of evaluation followed Zijp's work[11]. Although basically similar to Hughes' method, the evaluation of the cross section and the threshold energy was calculated using a least squares fit, so that the values give the best fit between the ideal threshold reaction and the actual response. If the response of the detector is expressed by

$$A = \int_0^\infty dE\ \sigma(E)\ \phi(E) \tag{4.3.11}$$

Then the effective cross section (σ_o) and the effective threshold energy (E_{eff}) are expressed as

$$\sigma_o \int_{E_{eff}}^{E_{max}} dE\ \phi(E) = \int_0^\infty dE\ \sigma(E)\ \phi(E), \tag{4.3.12}$$

or

$$\sigma_o = \frac{\int_0^\infty dE\ \sigma(E)\ \phi(E)}{\int_{E_{eff}}^{E_{max}} dE\ \phi(E)} \tag{4.3.13}$$

Zijp[11] evaluated σ_o and E_{eff} using three fission spectrum models, namely, the models of Watt[25], Cranberg and Frye[26], and Leachman.[27] Leachman's fission spectrum model gives a good approximation at lower energy, but it overestimates at higher energy, while Watt's, Cranberg and Frye models give a better approximation at higher energy. Since the

measurement used only three detectors, namely, In, Ni, and Al, and they covered the energy range between 1.4 MeV to 20 MeV, the values for σ_o and E_{eff} were taken from the results of the fission spectrum model of Cranberg and Frye, which is tabulated in Table 9.

In each foil detector, the measured flux is the integral flux, starting from the effective threshold energy up to maximum energy, which is assumed to be 20 MeV. Using three detectors with different threshold energies, the flux in between the threshold energy of two detectors can be evaluated. From Eq. (4.3.12)

$$\sigma_o \int_{E_{eff}}^{E_{max}} dE\ \phi(E) = \int_0^{\infty} dE\ \sigma(E)\ \phi(E). \qquad (4.3.14)$$

Let,

E_{thI} = effective threshold energy for detector number 1,

E_{thII} = effective threshold energy for detector number 2,

E_{thIII} = effective threshold energy for detector number 3,

Then,

$$\int_0^{\infty} dE\ \sigma(E)\ \phi(E) = \int_0^{E_{thII}} dE\ \sigma(E)\ \phi(E) + \int_{E_{thII}}^{E_{thIII}} dE\ \sigma(E)\ \phi(E)$$

$$+ \int_{E_{thIII}}^{\infty} dE\ \sigma(E)\ \phi(E) = \sigma_1 \int_{E_{thI}}^{E_{thII}} dE\ \phi(E) + \sigma_2 \int_{E_{thII}}^{E_{thIII}} dE\ \phi(E)$$

$$+ \sigma_3 \int_{E_{thIII}}^{E_{max}} dE\ \phi(E)\ , \qquad (4.3.15)$$

Table 9. The values of effective threshold energy and effective cross section.[11]

Type of Detector	Reaction	Effective Threshold Energy (MeV)	Effective Cross Section (mb)
In	$^{115}In(n,n')^{115m}In$	1.4	329.1
Ni	$^{58}Ni(n,p)^{58}Co$	2.7	395.1
Al	$^{27}Al(n,\alpha)^{24}Na$	7.1	57.56

where σ_1, σ_2, and σ_3 are evaluated from

$$\sigma_1 = \frac{\int_0^{E_{thII}} dE\ \sigma(E)\ \phi(E)}{\int_{E_{thI}}^{E_{thII}} dE\ \phi(E)}, \tag{4.3.16}$$

$$\sigma_2 = \frac{\int_{E_{thII}}^{E_{thIII}} dE\ \sigma(E)\ \phi(E)}{\int_{E_{thII}}^{E_{thIII}} dE\ \sigma(E)}, \tag{4.3.17}$$

and

$$\sigma_3 = \frac{\int_{E_{thIII}}^{\infty} dE\ \sigma(E)\ \phi(E)}{\int_{E_{thIII}}^{E_{max}} dE\ \sigma(E)\ \phi(E)}. \tag{4.3.18}$$

Let us look at In as a fast neutron detector. We can split the cross-section into three regions, namely (1.4 - 2-7)MeV, (2.7 - 7.1)MeV, and (7.1 - 20.0)MeV. Therefore the activation due to fission spectrum neutrons, can be written as :

$$\sigma_o^{In}\int_{1.4}^{20} \phi(E)\ dE = \sigma_1^{In} \int_{1.4}^{2.7} \sigma(E)dE + \sigma_2^{In} \int_{2.7}^{7.1} \phi(E)dE + \sigma_3^{In} \int_{7.1}^{20} \phi(E)dE\ . \tag{4.3.19}$$

Using the same method for Ni and Al, we get

$$\sigma_o^{Ni} \int_{2.7}^{20} \phi(E)dE = \sigma_2^{Ni} \int_{2.7}^{7.1} \phi(E)dE + \sigma_3^{Ni} \int_{7.1}^{20} \phi(E)dE \tag{4.3.20}$$

and

$$\sigma_o^{Al} \int_{7.1}^{20} \phi(E)dE = \sigma_3^{Al} \int_{7.1}^{20} \phi(E)dE \tag{4.3.21}$$

The values for σ_1^{Ni}, σ_1^{Al}, and σ_2^{Al} are

$$\sigma_1^{Ni} = \sigma_1^{Al} = \sigma_2^{Al} = 0.$$

Therefore we can write Eqns. 4.3.19, 4.3.20 and 4.3.21 in matrix form as

$$\begin{pmatrix} \sigma_1^{In} & \sigma_2^{In} & \sigma_3^{In} \\ 0 & \sigma_2^{Ni} & \sigma_3^{Ni} \\ 0 & 0 & \sigma_3^{Al} \end{pmatrix} \begin{pmatrix} \phi_1 \\ \phi_2 \\ \phi_3 \end{pmatrix} = \begin{pmatrix} \sigma_0^{In}(\phi_1 + \phi_2 + \phi_3) \\ \sigma_0^{Ni}(\phi_2 + \phi_3) \\ \sigma_0 \ \phi_3 \end{pmatrix} \tag{4.3.22}$$

The right hand part of equation (4.3.22) are the results of the measurements for each detector. The unknown values are ϕ_1,ϕ_2, and ϕ_3, which correspond to the energy ranges 1.7-2.7, 2.7-7.1, and 7.1-20 MeV, respectively. Therefore we have three equations with 3 unknowns, which will give a unique answer.

To evaluate Eqs. 4.3.16-4.3.18, the data of Zijp[11] were used, and the integration was calculated using Simpson's rule. The average cross-sections for Indium, Nickel and Aluminum are shown in Table 10. The measurement of the integrated neutron flux using the foil detectors, are substituted into the RHS of Eq. (4.3.22). The solutions are the fluxes in the interval between two successive threshold energies. The solutions are compared with the fission spectrum, which is normalized with the result in energy interval 7.1-20 MeV. The results are shown in Table 11. The maximum error associated with each measured value is about 3%. The measured fluxes are higher in the lower energy intervals than are the fluxes calculated from the fission spectrum. A reason for this difference is due to the scattering by the graphite reflector. Some of the neutrons with higher energy are scattered by the graphite reflector to the detector at a lower energy. As a result the flux in the lower energy interval is increased. A second possibility is due to the scattering by Zirconium Hydride in the fuel and also some scattering by water. Since hydrogen is an effective moderator, the contribution to lower energies will be small. As a comparison, from the result of West[8], for TRIGA Mark II reactor with 76 fuel element at water and fuel temperature of 23^{o} C and a fueled F-ring, the fast neutron flux in the energy interval; 1.35 to 3.68, MeV is 9.95×10^{11} (cm^{-2} sec^{-1}) at 250 kW of power. The KSU TMII at present time has 79 fuel elements (Loading II-9), and the fuel element is type 504 which has 38 grams of U-235. In the West's calculation the fuel element has 36 g of U-235, with aluminum cladding.

For the geometrical distribution of fast neutrons, the control rod does not have any effect, because boron has a large absorption cross-section for thermal neutrons. Hence, the deviation in the distribution

Table 10. The Average Cross Section of In, Ni and Al.

Detector	Average Cross Section (barn)		
	(1.4-2.7) Mev	(2.7-7.1) Mev	(7.1-20) Mev
In	0.14289	0.34779	0.28070
Ni	0	0.13591	0.60693
Al	0	0	0.57560

Table 11. Fast neutron spectrum at the end of the outer tube (cm^{-2} sec^{-1}).

Position	Energy 1.4-2.7 MeV Measured	Energy 1.4-2.7 MeV Fission Spectr.	Energy 2.7-7.1 Measured	Energy 2.7-7.1 Fission Spectr.	Energy 7.1-20.0 Measured	Energy 7.1-20.0 Fission Spectr.
1	1.458×10^{12}	8.844×10^{11}	1.106×10^{12}	7.056×10^{11}	3.061×10^{10}	3.061×10^{10}
2	1.333×10^{12}	9.325×10^{11}	1.171×10^{12}	7.439×10^{11}	3.227×10^{10}	3.227×10^{10}
3	1.374×10^{12}	9.927×10^{11}	1.139×10^{12}	7.920×10^{11}	3.436×10^{10}	3.436×10^{10}
4	1.158×10^{12}	9.079×10^{11}	1.072×10^{12}	7.243×10^{11}	3.142×10^{10}	3.142×10^{10}
5	1.787×10^{12}	9.561×10^{11}	1.020×10^{12}	7.628×10^{11}	3.309×10^{10}	3.309×10^{10}
6	1.497×10^{12}	9.013×10^{11}	1.169×10^{12}	8.079×10^{11}	3.505×10^{10}	3.505×10^{10}
7	1.223×10^{12}	8.085×10^{11}	1.157×10^{12}	7.089×10^{11}	3.075×10^{10}	3.075×10^{10}
8	1.335×10^{12}	9.067×10^{11}	1.111×10^{12}	7.233×10^{11}	3.138×10^{10}	3.138×10^{10}

is due to the burnup of the fuel element. The fuel elements close to the control rod have very different burnup distribution along the axial direction. As a consequence, the neutron flux distribution will deviate also. The fast neutron flux distribution for both vertical and horizontal directions in the beamport roughly reflected this deviation in the core flux. Figures 20 and 21 show the fast neutron distribution in vertical and horizontal direction, respectively.

The fast neutron spectra in the specimen chamber were measured by the same method using three threshold detectors. The results are shown in Table 12 and compared to the fission spectrum from the Cranberg and Frye model normalized to the measured flux in the energy interval 7.1-20 MeV.

The measured spectrum for the energy interval 2.7-7.1 MeV was lower than the theoretical spectrum. This is due to the absorption by Fe-56, Cr-50, and Ni-58 in the end cover of outer tube. The end cover is made from stainless steel and is 4 mm thick. The main compositions of stainless steel type 304 are 72% Fe, 19% Cr, and 9% Ni. Fe-56 (95.6% natural abundance) reacts with a fast neutron and produces Mn-56 with a half life 154.5 minutes[13,16]. The reaction has effective cross section of 130 mbarn and a threshold energy of 2.95 MeV. The peak of the cross-section is around 6 MeV with the magnitude 250 mbarn. For Cr-50, the threshold energy is 4.5 MeV and the effective cross section 57 mbarns. Hence, in the region 2.7-7.1 MeV, the flux is decreased due to absorption by Fe-56, Cr-50, and Ni-58.

4.3.4 Gamma Ray Dose Rate in Specimen Chamber[7]

The radiation field in the chamber is a mixture of fast neutrons and prompt fission gammas. Actually there are also thermal neutrons, but the

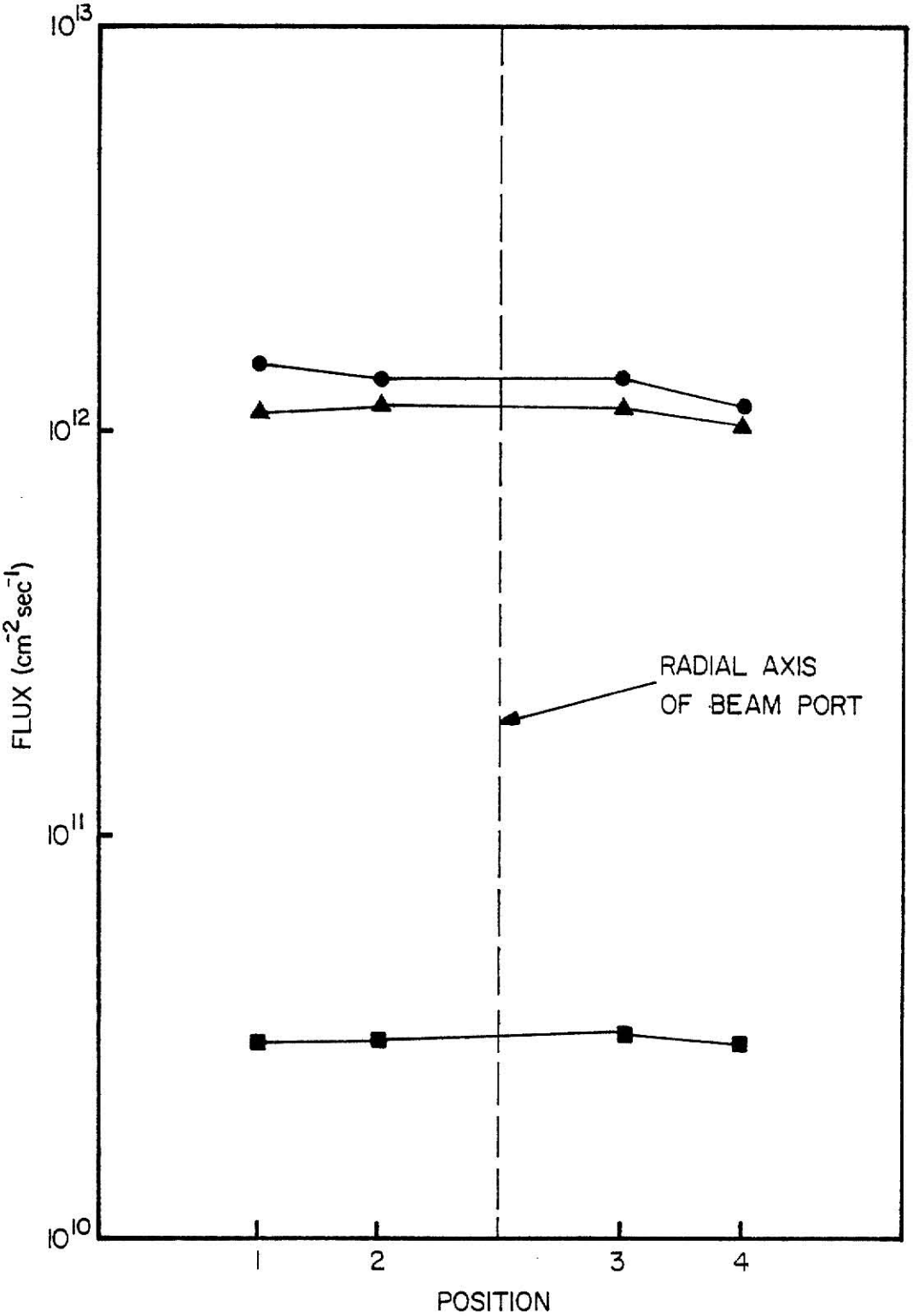

Fig. 20. Measured Fast Neutron Flux Distribution in the Vertical Direction

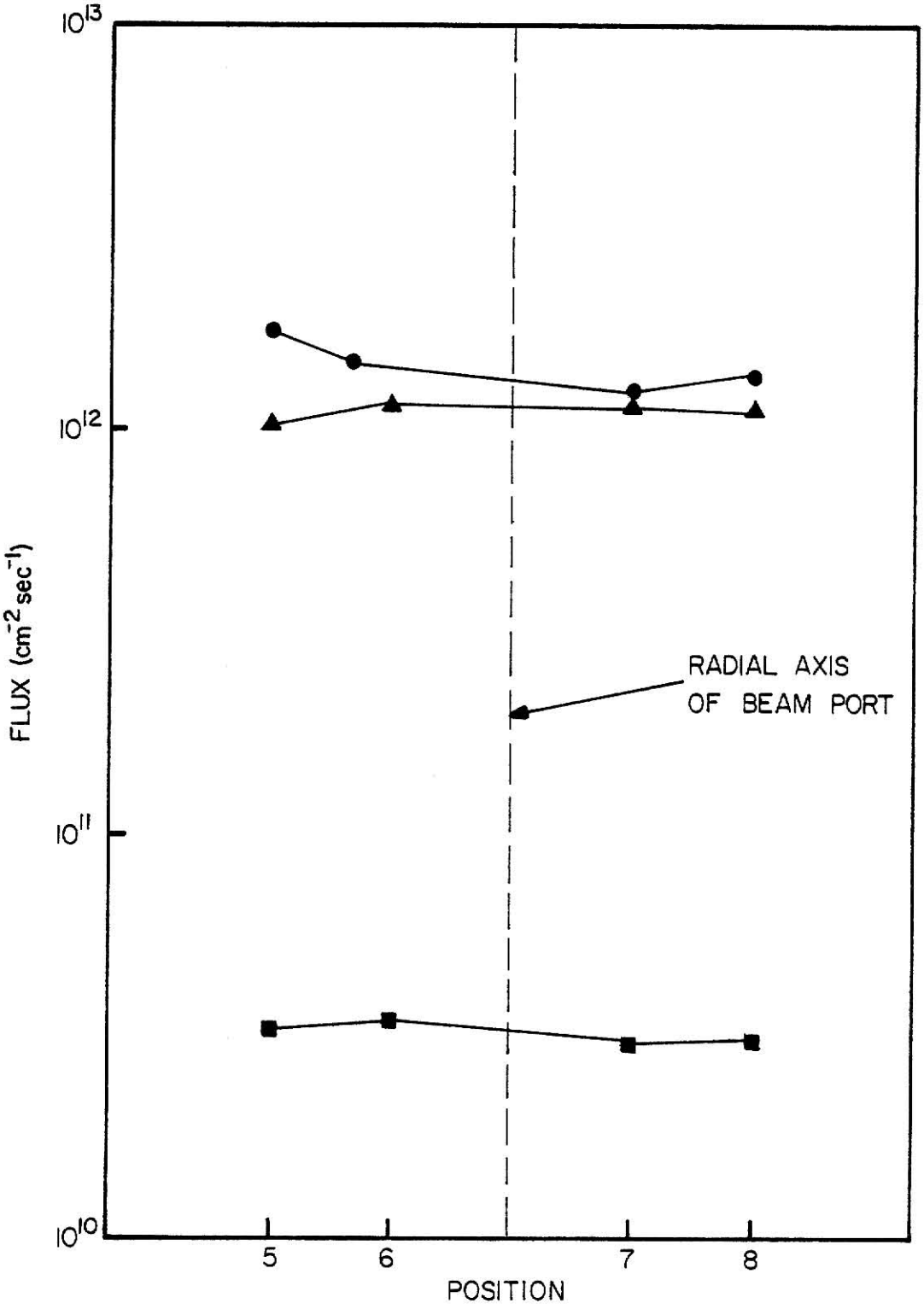

Fig. 21. Measured Fast Neutron Flux Distribution in the Horizontal Direction

Table 12. Fast neutron spectrum at the specimen chamber.

Energy Interval (MeV)	Measured	Fission Spectrum
1.4 - 3.7	$8.666 \times 10^{10} \pm 9.35 \times 10^{9}$	8.459×10^{10}
3.7 - 7.1	$3.405 \times 10^{10} \pm 5.69 \times 10^{9}$	6.75×10^{10}
7.1 - 20.0	$2.928 \times 10^{9} \pm 7.55 \times 10^{7}$	2.928×10^{9}

density is much smaller than the fast neutron density. The 2 mm thick cadmium sheet absorbed approximately 99.99% of the thermal neutrons.

As in the case of the fast neutron flux, there is no accurate information on the dose rate of gamma rays in the beamport. The data, which is available, is the approximate dose rate at ring-F of the core. If the reactor is operated at full power, the approximate dose rate is 10^4 rad/sec. In order to calculate the dose rate at specimen chamber, the gamma flux is assumed to be isotropic. Then the dose rate at the specimen chamber can be calculated by geometrical attenuation. The source has a circular shape, the diameter equal to the radius of the beamport.

The gamma flux can be calculated from the dose rate at the F-ring using the relation

$$\phi^{+} = \frac{D}{E\mu_k \rho^{-1}} \tag{4.3.23}$$

where

ϕ^{+} = isotropic gamma ray flux

E = the gamma energy for prompt fission gamma ($\simeq$1MeV),

μ_k = absorption coefficient of air,

ρ = density of air, (g/cm^3)

D = dose (rad)

The gamma flux at specimen position is

$$\phi(s) = \int_0^{\Theta_{max}} \phi(\Theta) \sin \Theta \, d\Theta. \tag{4.3.24}$$

where

$$\phi(\Theta) = \frac{\phi+}{2\pi}$$

Θ_{max} = maximum angle between axis of the beamport to the line connecting the specimen position and the edge of the beamport which is adjacent to the core.

The dose rate at the specimen position, if the reactor is operated at full power is,

$$D(S) = E\ \phi(s)\ (\mu_k \rho^{-1}) \qquad (4.3.25)$$

$$\simeq 50 \text{ krad/hr.}$$

The gamma ray intensity rate after reactor shut-down is expressed by[23]:

$$P\gamma(To,Ts) = 2.19 \times 10^{11}\ P\left[Ts^{-.2} - (Ts + To)^{-0.2}\right] \ \{MeV/sec\} \qquad (4.3.26)$$

Where

$P\gamma(To,Ts)$ is total energy emitted per unit time

P = Reactor power {Watt}

Ts = Time after shutdown

To = Time the reactor in operation.

The gamma ray spectrum from fission product has an empirical relation as:

$$n(E) = 6.0 \exp(-1.1E) \quad \{MeV^{-1}\}\ , \qquad (4.3.27)$$

E is energy (MeV)

and the average energy can be calculated as:

$$\bar{E} = \frac{\int_0^{3.5} En(E)dE}{\int_0^{3.5} n(E)dE} = 0.846 \quad \text{MeV} \qquad (4.3.28)$$

The upper limit of fission product gamma ray is 3.5 MeV[24]. Using Eqs. (4.3.26) and (4.3.28) the integrated dose at the sample position for one hour after shutdown when the reactor has been operated at 225 kW for 1 hour, is ≃ 3 krad.

5.0 IRRADIATION OF LiF

To show the effect of fast neutron irradiation, LiF crystals were irradiated in the irradiation chamber, and also in the Co-60 irradiator. The effect of gamma rays on the result of irradiation in the chamber, can be calculated with the help of the previous calculation in gamma radiation. This estimated absorbance is subtracted from the absorbance change produced by the combined fast neutron and gamma dose in the irradiation chamber. The difference is the estimate of absorbance change to fast neutrons. Two sets of LiF were irradiated. The first set were irradiated at room temperature with the neutron fluence varying from 5×10^{13} to 4×10^{14} (cm^{-2}). The second series were irradiated at a fixed neutron fluence, (10^{14} (cm^{-2})) and the sample temperature was varied from room temperature up to 500° C (773° K).

The change in absorbance due to gamma irradiation is shown in Table 13 and Fig. 22. The approximate dose rate due to prompt fission gammas is 50 krad/hr. Hence, the change in absorbance due to the prompt fission gammas is approximately 0.27 (cm^{-1}) at 5 eV.

The first set of samples were irradiated in the chamber at room temperature. The neutron fluence was varied from 5×10^{13} (cm^{-2}) up to 4×10^{14} (cm^{-2}). The results corrected for the gamma dose can be

Table 13. Change of absorbance in pure LiF crystal due to gamma irradiation.

Dose (Krad)	Change of Absorbance at 5 eV (cm^{-1})
100	0.65
200	1.18
300	1.41
400	2.06
500	2.45

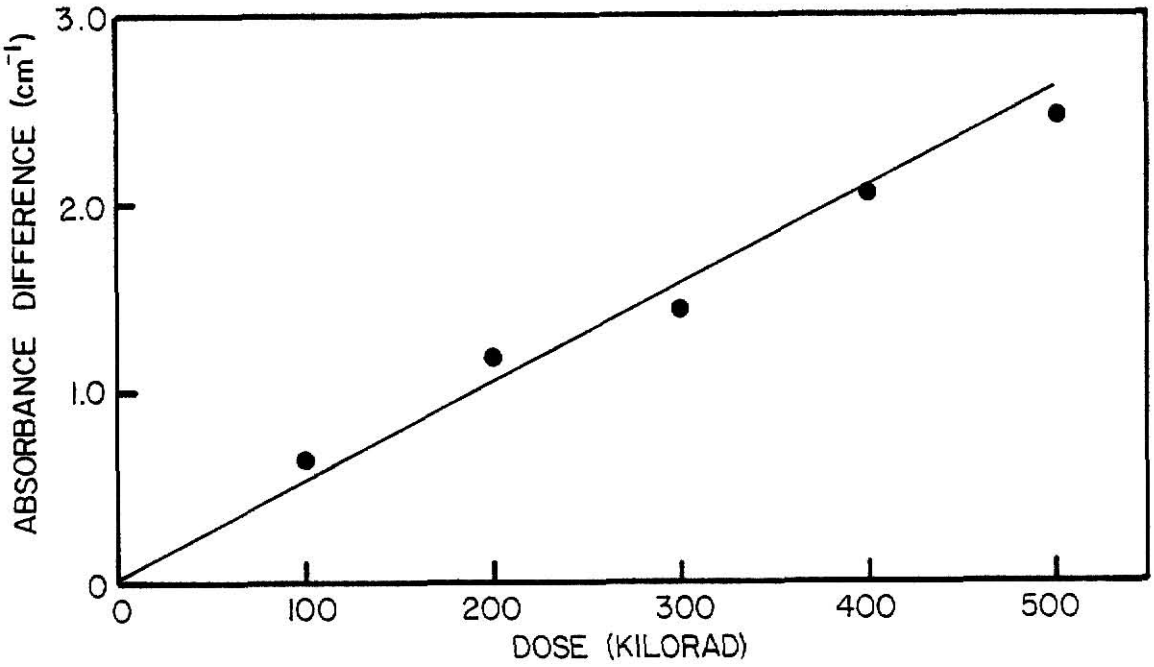

Fig. 22. Change of Absorbance vs Gamma Dose

seen in Table 14 and Fig. 23. It can be seen from Fig. 23 that the change in absorbance is still linear up to the fluence 4×10^{14} (cm^{-2}).

The second set of LiF samples were irradiated at a fixed neutron fluence, i.e., 10^{14} (cm^{-2}), and the sample temperatures were varied from room temperature up to 500 C. The reactor was brought to full power after the desired temperature in the specimen chamber was reached. The time needed to get to the maximum temperature was approximately 20 minutes after the heater was energized. The results are shown in Table 15 and Fig. 24. The change in absorbance at 5 eV is constant up to 150 C, then decreases sharply and is constant from 200 C to 400 C. The change in absorbance is zero when the sample is irradiated at 500 C.

It should be noted that the heater was turned off at the same time that the reactor was shut down. The samples were kept overnight in the specimen chamber. Hence, the sample experienced a gradual decrease in temperature and also were exposed to the fission product gammas.

The fast neutrons will undergo elastic scattering reaction with lithium and flouride ions in the lattice, producing both positive and negative ion vacancies, interstitials and F-centers. In alkali halides, Frenkel defects and Schottky defects are mobile. The motion of the interstitial halogen atom could lead to a reaction with an F-center. In this reaction, the F-center would be destroyed. The motion of any defect is governed by the probability that the defect can move to an adjacent site. The probability of a defect moving is given by the equation[21].

$$P = \nu_o \, e^{-E_A/kT} \tag{5.1}$$

Table 14. Change of absorbance at room temperature due to fast neutron irradiation.

Sample Number	Fluence (cm^{-2})	Change of Absorbance by Neutron (cm^{-1})
1	5×10^{13}	1.37
2	5×10^{13}	1.21
3	1×10^{14}	1.40
4	2×10^{14}	1.66
5	2×10^{14}	1.48
6	4×10^{14}	1.72
7	4×10^{14}	2.16

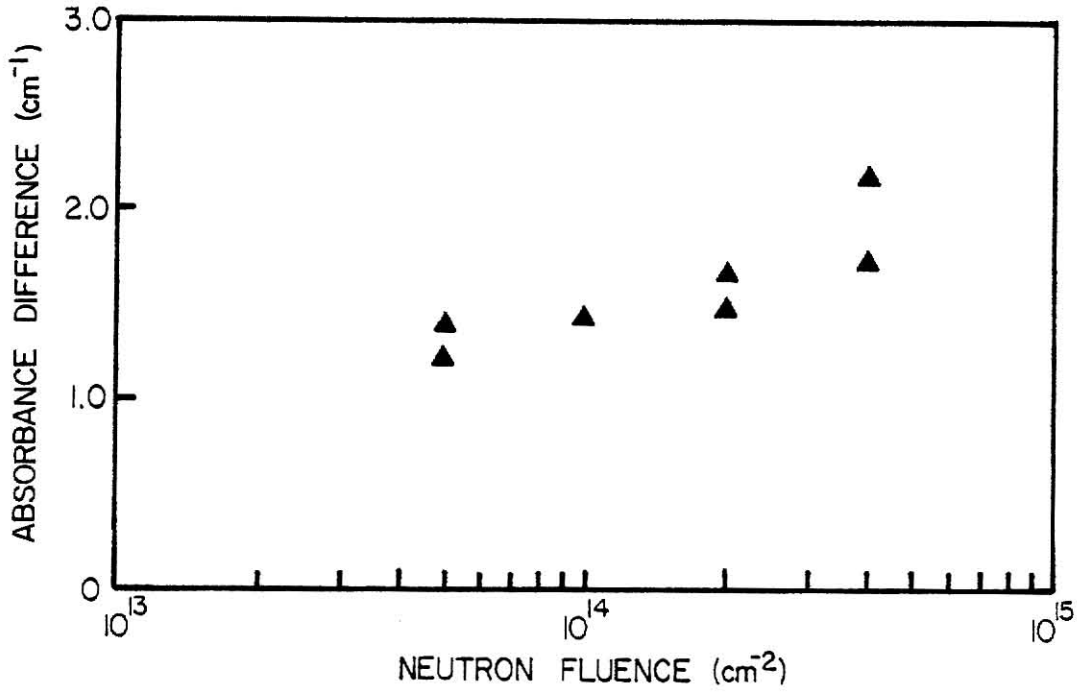

Fig. 23. Change of Absorbance vs Neutron Fluence

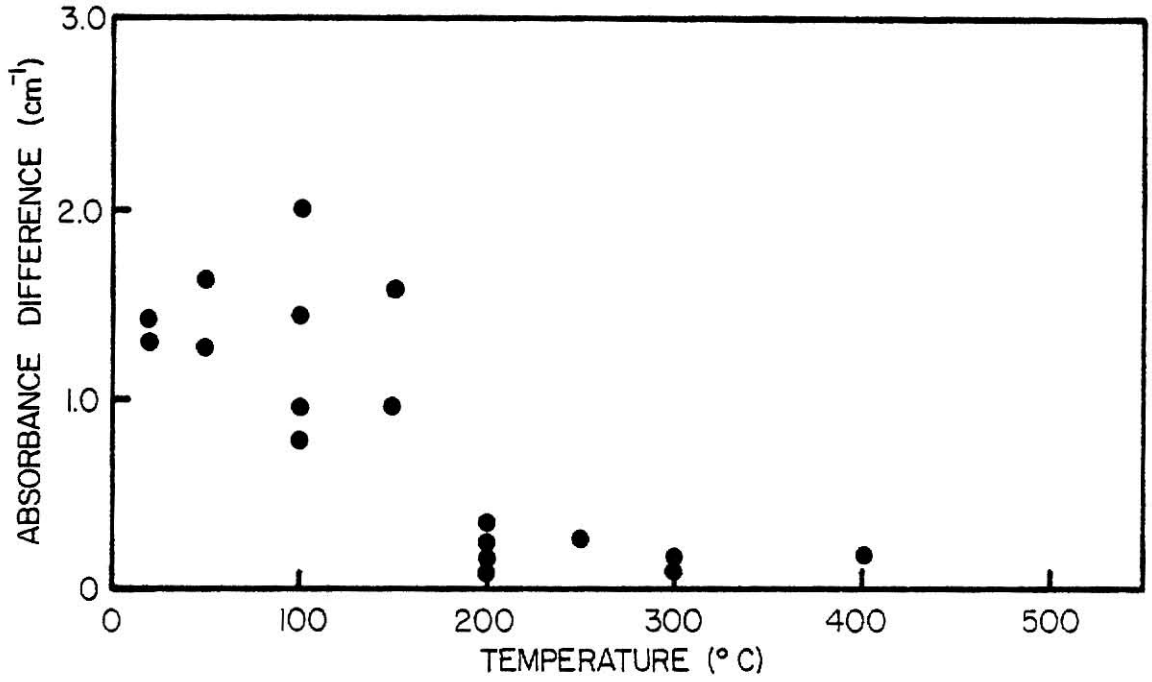

Fig. 24. Change of Absorbance vs Temperature of Irradiation Neutron Fluence: 10^{14} (cm^{-2})

Table 15. Change of absorbance at 5 eV as a function of temperature at constant fluence (10^{14} cm^{-2}).

Number of Sample	Temperature of Irradiation (^{o}C)	Change in Absorbance (cm^{-1})
1	Room Temp.	1.4
2	Room Temp.	1.28
3	50	1.61
4	50	1.26
5	100	1.98
6	100	1.42
7	100	0.93
8	100	0.77
9	150	1.56
10	150	0.93
11	200	0.14
12	200	0.08
13	200	0.33
14	200	0.23
15	250	0.25
16	300	0.09
17	300	0.16
18	400	0.16
19	400	0.16
20	500	0
21	500	0

where

ν_o = the jump frequency and is of the order 10^{13} Hz

E_A = energy of activation

k = Boltzmann constant

T = absolute temperature.

The energy of activation for the motion of a Frenkel defect in LiF is 1.3 eV[22]. This value of the activation energy indicates that at 300 K this defect could move. As the temperature increases the probability for movement of this defect increases. The probability of motion at 473 K is about eight orders of magnitude larger than the probability at 300 K and is about thirteen orders of magnitude larger at 773 K. The increased mobility of neutron produced interstitials at elevated temperatures can annihilate the F-center. After the reactor is operated for one hour at power 225 KW, the approximate dose for the first hour after shut down is 3 krad. This dose will not cause a signigicant change in LiF, since the results in Table 13 show that for a dose of 100 krad, the change in absorbance is 0.65 $\{cm^{-1}\}$.

6.0 CONCLUSION

From four experiments which were performed before and after the installation of the irradiation chamber, the following conclusions can be drawn.

1. The maximum temperature on the beamport liner, when the heater is operated at a current of 6 Amps or power ~200 watts, is below 50 C. This means that the possibility of the deterioration of the concrete by dehydration is prevented. The Kansas State University Safeguards Committee required that at any time during the operation of the heater inside the beamport, the temperature of the concrete shielding could not exceed 50 C.

2. The radiation dose rate for both gamma and neutron in the surrounding area of the beamport, when the irradiation chamber is installed and operated at full power, is below 2 mrem/hr. However in front of the center of the beamport, in a cross-sectional area 3.2 x 3.2 cm, the total radiation dose rate is higher than 10 mrem/hr. Hence, in a distance about 2 m beside the beam port, a worker could work continuously while the heater is operating without showing a radiation dose rate higher than 2 mrem/hr. A reminder sign and rope are necessary to be installed surrounding the radial piercing beamport, when the irradiation chamber is installed.

3. The fast neutron spectrum in the specimen chamber similar to the fission spectrum for energy above 1.4 MeV, according to the results of the three threshold detectors, i.e., In, Ni, and Al. The

integral flux from energy 1.4 to 20 Mev is in the order of 10^{11} (n/cm^2 sec), if the reactor is operated at 250 kW.

4. The thermal neutron flux in the specimen chamber is of the order of 4×10^8 (n/cm^2 sec). When the reactor is operated at 250 kW.

5. The gamma dose rate in the specimen chamber due to the prompt fission gamma is approximately 50 krad/hr, at 250 kW.

6. The specimen chamber can be operated up to 600°C.

7. The formation of F-center was linear up to the fluence of 5×10^{14} (n/cm^2) at room temperature. The absorbance of the F-center was constant up to 200°C, and then decreased rapidly and was constant between 250° to 450°C. The absorbance of the F-center was zero at 500 C. The absorbance of the F-center was zero at 500 C.

REFERENCES

1. Kouts, H., "The Uses and Potentialities of Research Reactors," Proceedings of the Third International Conference on the Peaceful Uses of Atomic Energy, Vol. 7, United Nations, 1965.

2. Simnad, M. T., and R. H. Chesworth, "TRIGA Research Reactor Experimental Instrumentation," Proceedings of a Symposium on Irradiation Facilities for Research Reactor Teheran, November, 1972, Paper IAEA-SM-165/18.

3. GA-2627 (Rev.), "TRIGA Mark II Reactor, General Specifications and Description," March, 1964.

4. Handbook of Tables for Applied Engineering Science, Bolz, R. E., and G. C. Tuve, Editors, CRC Press, 2nd Edition, 1973, page 117.

5. GA-3399, "250 kW TRIGA Mark II Pulsing Reactor Mechanical Maintenance and Operating Manual," August, 1962.

6. Docket No. 50-188.

7. Docket No. 50-188, Amendment 3.

8. West, G. B., "Calculated Fluxes and Cross Section for TRIGA Reactors," GA-4361, 1963.

9. David, H. S., and A. M. Asce, "Thermal Consideration in the Design of Concrete Shields," Journal of the Structural Division, Proceedings of the Society of Civil Engineers, September, 1958, pp. 1775-1 - 1775-25.

10. Lamarsh, J. R., "Introduction to Nuclear Reactor Theory," Addison-Wesley Publishing Co., 1972, p. 97.

11. Zijp, W. L., et al., "Compilation of Evaluated Cross Section Data in Fast Neutron Metrology," RCN-196, October, 1973.

12. Beckurtz, K. H., and K. Wirtz, "Neutron Physics," Springer-Verlag, New York Inc., 1964, pp. 233-340.

13. Shultis, J. K., "Instruction Manual Reactor Technology Laboratory, NE 695," 1974, Department of Nuclear Engineering, Kansas State University (unpublished).

14. Lederer, C. M., et al., "Table of Isotopes Sixth Edition," John Wiley and Sons, Inc., 1967.

15. 1977 Annual American Society of Testing Materials Part 45, E-261-A7 266-77, E-481-73T, E482-76.

16. Hughes, D. J., "Pile Neutron Research," Addison-Wesley Publishing Corp., 1953, pp. 93-102.

17. Faw, R. E., Private Communication.

18. Zijp, W. L., "Review of Activation Method for the Determination of Fast Neutron Spectra," RCN-37, May, 1965.

19. Billington, D. S., and J. H. Crawford, Jr., "Radiation Damage in Solids," Princeton University Press, 1961, pp. 249-265.

20. ANL-5800, "Reactor Physics Constant," Argonne National Laboratory, July, 1963, pp. 668-672.

21. C. Kittel, "Introduction to Solid State Physics," J. Wiley and Sons, Inc., New York, 1971, 3rd Edition.

22. J. H. Crawford and L. N. Slifkin (Ed.), "Point Defects in Solids," Plenum Press, New York, 1972., Vol. 1, General and Sonic Crystals.

23. Blizard, E. P., (Ed.) "Reactor Handbook: Vol. III, Part B, Shielding, Second Edition," Interscience, New York, 1962.

24. Rockwell, T., "Reactor Shielding Design Manual," D. Van Nostrand Co., Inc., Princeton, New Jersey, 1956.

25. Watt, B.E., "Energy Spectrum of Neutrons from Thermal Fissions of U-235," Physical Review 87 (1952), p. 1037.

26. Cranberg, L., Frey, G., Nueson, N., and Rosen, L., "Fission Neutron Spectrum of U-235," Physical Review, 103 (1956), 662.

27. Leachman, R. B., "Determination of Fission Quantities of Importance to Reactors," Proc. Int. Conf. on Peaceful Uses of Atomic Energy, Geneva, 1955, Vol. 2 (1956), p. 193.

28. Price, W. J., "Nuclear Radiation Detection," Second Edition, McGraw-Hill Book Co., New York, 1964, p. 132.

APPENDIX I

Experiment No. 41

K.S.U. TRIGA Mk II Nuclear Reactor Facility

Operation of an Electrically Heated Irradiation Chamber in the Radial Piercing Beam Port

Objective

The purpose of the experiment is to install and operate an electrical heater in the radial piercing beam port of the KSU TRIGA Mk II Reactor. Thedevice is purged, using nitrogen, helium or carbon dioxide, and incorporates a heating element up to 200 W, permitting irradiation of specimens at temperatures up to $1000^{o}K$.

Background Information

The main objective of this experiment is to establish an irradiation facility which will give a fast neutron radiation field and elevated temperatures. A heater, made of nichrome wire of 1 mm diameter, is wound on a hollow ceramic holder. The temperature inside the holder can be adjusted by means of varying the voltage applied to the heater.

Since the energy distribution of the neutrons from the reactor core contain thermal, intermediate and fast neutrons, a cadmium sheet will be installed in front of the heater in order to absorb thermal neutrons.

Heater Design

A diagram showing the placement of the heater in the radial piercing (fast) beam port is shown in Fig. 1. The assembled system has three main components; a heater structure, a beam port plug and a sample holder. To facilitate installation and pre-installation testing, the components are assembled into one unit before placement in the beam port.

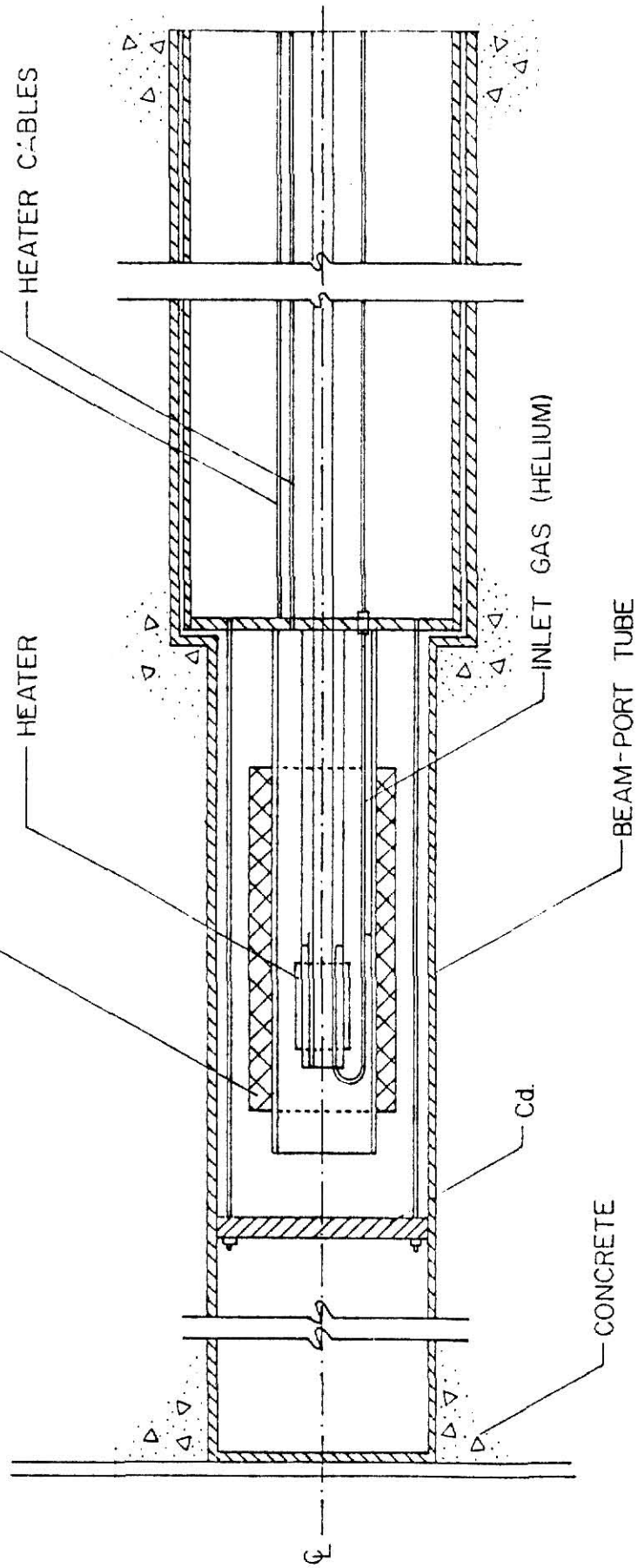

Fig. 1. DIAGRAM OF FAST NEUTRON IRRADIATOR AT ELEVATED TEMPERATURES POSITION RADIAL PIERCING BEAM-PORT

Heater Structure

The purpose of the heater is to allow irradiation of specimens at temperatures up to 1000°K. The heater structure is made up of four parts; a heating element, a heater support, an inner tube, and an outer tube.

The heating element is shown in Fig. 2. It is made from 1-mm diameter nichrome wire wound on a porcelain holder. To minimize radiation heat losses two layers of 2 mm thick asbestos sheet are wrapped around the heater and held in place by Nichrome wire.

The heating element, on its support structure, is illustrated in Fig. 3. The support structure not only supports the heating element, but also conducts heat axially, thereby more evenly heating the specimens. The support structure is made from type 304 stainless steel. The heating elements are held in place by a threaded ring, made of 304 stainless steel.

The overall heater structure, is illustrated in Fig. 4. The inner and outer tubes, made of low-carbon steel, serve to shield the beam port from direct radiant heating. As shown in Fig. 1, the inner tube is wrapped with a 2 cm thickness of glass wool.

The 1mm thick cadmium absorber is attached to the end of the outer tube as shown in Fig. 1. The distance from the cadmium absorber to the reactor tank is 18.4 cm.

Beam Port Plug

The beam-port plug, previously constructed for use in the KSU TRIGA Reactor Facility, is 150 cm long and 19.7 cm diameter, made of steel and concrete. The plug has an axial square duct, of dimensions 3.1 x 3.1 cm and three small circular ducts of dimensions 0.3 cm diameter used for purge gas lines, heater cables, and thermocouple leads. The axial ducts are used for insertion of the sample holder.

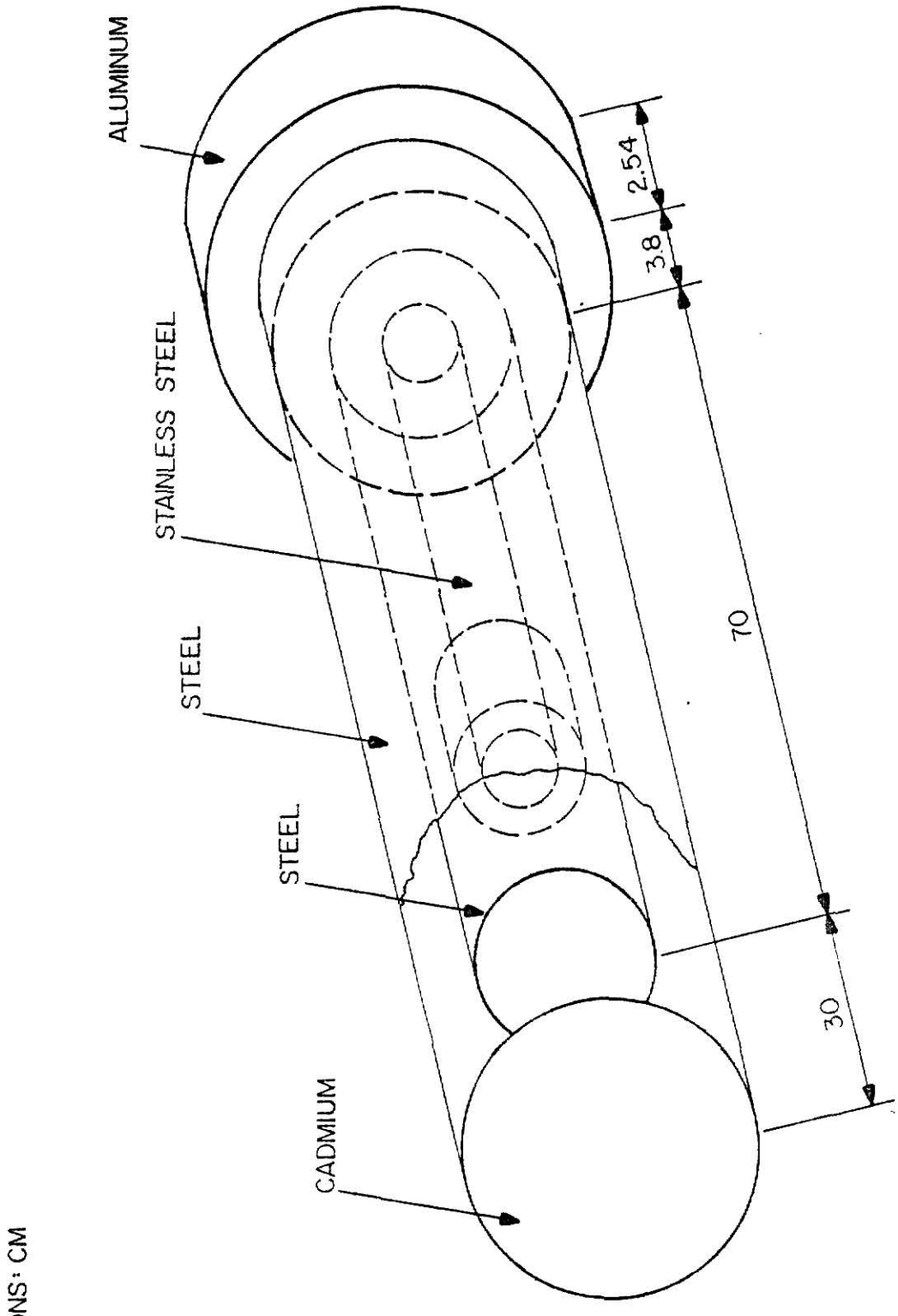

Fig. 2. Heater Structure

THIS BOOK IS OF POOR LEGIBILITY DUE TO LIGHT PRINTING THROUGH OUT IT'S ENTIRETY.

THIS IS AS RECEIVED FROM THE CUSTOMER.

DIMENSIONS : CM

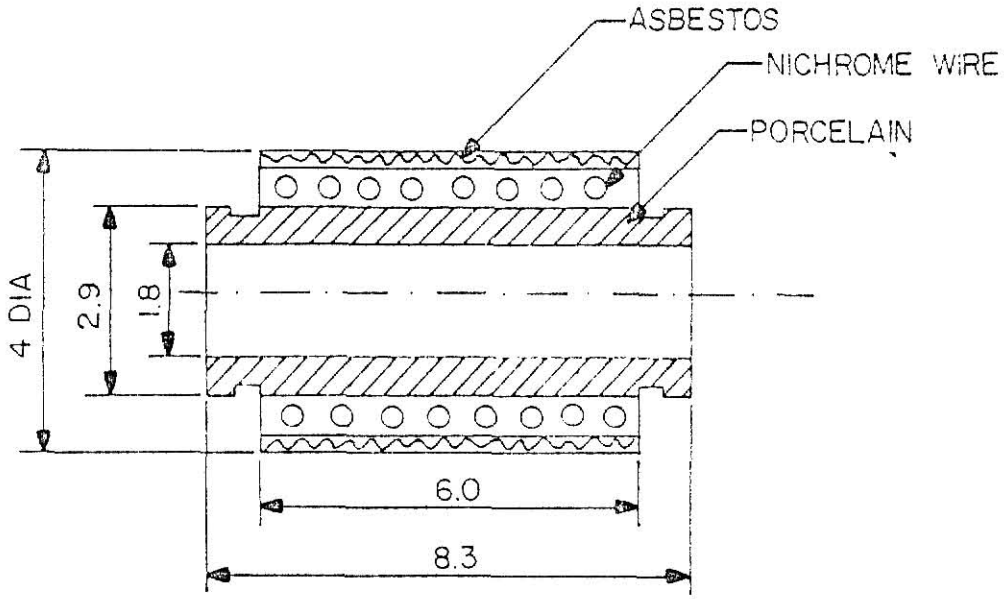

Fig. 3. Heating Element

DIMENSIONS : CM

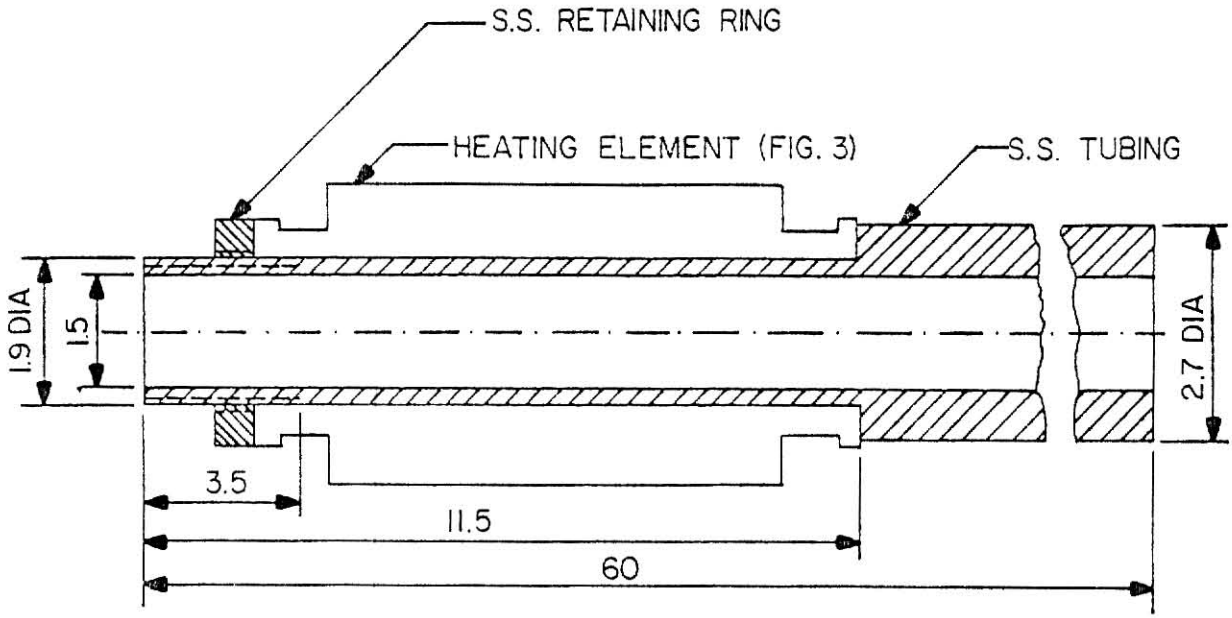

Fig. 4. Heater Support

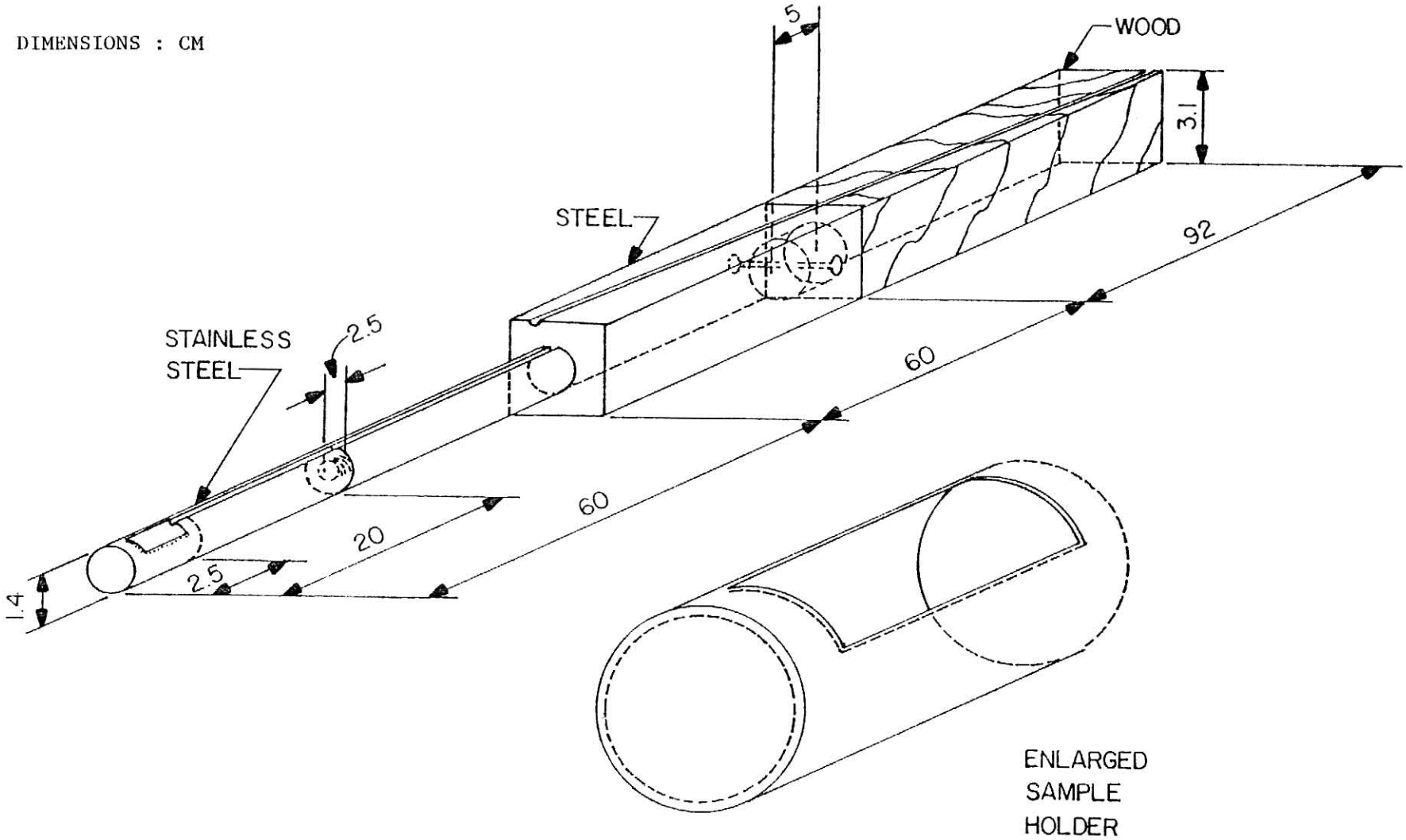

Fig. 5. Sample Holder Assembly

Sample Holder

The sample holder assembly is illustrated in Fig. 5. That portion of the sample holder which is positioned within the heater structure is constructed of type 304 stainless steel. That portion of the sample holder positioned within the beam port plug is made of a 60 cm length of low carbon steel, followed by a 92 cm length of wood. The sample holder itself is in the form of a hollow cylinder, and will accept samples up to 1 cm in diameter and up to 3 cm in length.

Safety Analysis

Fire

Except for the wooden moderator in the sample holder, positioned deep within the beam port plug, none of the construction materials are flammable.

Reactivity

The cadmium absorber will be positioned in the fast beam port, far from the reactor core. In such geometry, that the reactivity effect of the absorber is negligible.

Installation

The heater structure will be assembled as a unit outside the reactor and then installed following the procedures previously developed for installation of a beam port.

After installation, connection will be made for the sample heater, purge gas, and three thermocouples.

Heater Operations

The heating element is supplied with alternating current controlled by a variable transformer. Supply voltage and current will be monitored to assure that the heater operates at a power of no more than 200 W.

The temperature inside the assembly will be monitored by thermocouples at three positions; these are 1) the sample, 2) outside the outside cylinder, and 3) outside the glass wool. At the sample, a Chromel-Alumel thermocouple will be used. At the two other positions, Iron-Constantan thermocouple, will be used.

Purge Gas Monitoring

The purge gas flow rate during operation should be approximately 500 cm^3/min. The purge gas flow rate will be adjusted to assure that the beam port liner temperature does not exceed $50^{o}C$.

Radiation Monitoring

During installation of the generator, standard radiation protection procedures will be followed. During operation, radiation levels external to the reactor will be monitored; radiation or high-radiation areas will be posted and controlled according to requirements of 10CFR20.

Test Procedures

Preliminary Test

1. Reported here are results of tests of heater operation performed in the beam plug storage channel in the south wall of the lower reactor bay. Temperatures were measured at three locations:

1) At the sample location using Chromel-Alumel thermocouple.

2) Outside the outer tube of the heater structure, measured using an Iron-Constantan thermocouple.

3) Inside the beam plug storage liner, measured using an Iron-Constantan thermocouple.

The applied voltage was 30 volts, and heater current was 6 A. Results are illustrated in Fig. 6. The temperature of beam plug storage channel liner was 44°C after 135 minutes of heating and 500 cm^3/min nitrogen purge. From Davis, and Asce†, it is shown that neither the structural strength nor the water content of concrete will change significantly when the concrete is heated to 100°C. Hence, from the results of these measurements, the liner temperature will not endanger the properties of concrete from the points of view of either structural properties or nuclear properties.

2. The neutron spectrum distribution at the location of the cadmium filter has been measured using foil detectors. It was measured in 8 locations, around the centerline of the beam port and the results are tabulated as follows.

†Davis, H. S. and A. M. Asce, "Thermal Consideration in the Design of Contrete Shields, Journal of the Structural Design Proceedings of the American Society of Civil Engineers, paper 1755, Sept. 1958.

Fig. 6. Temperature vs Heating Time in the Beamport Storage Hole

Current: 6 A

Voltage: 6 A

Coolant: Helium (500 ml/min)

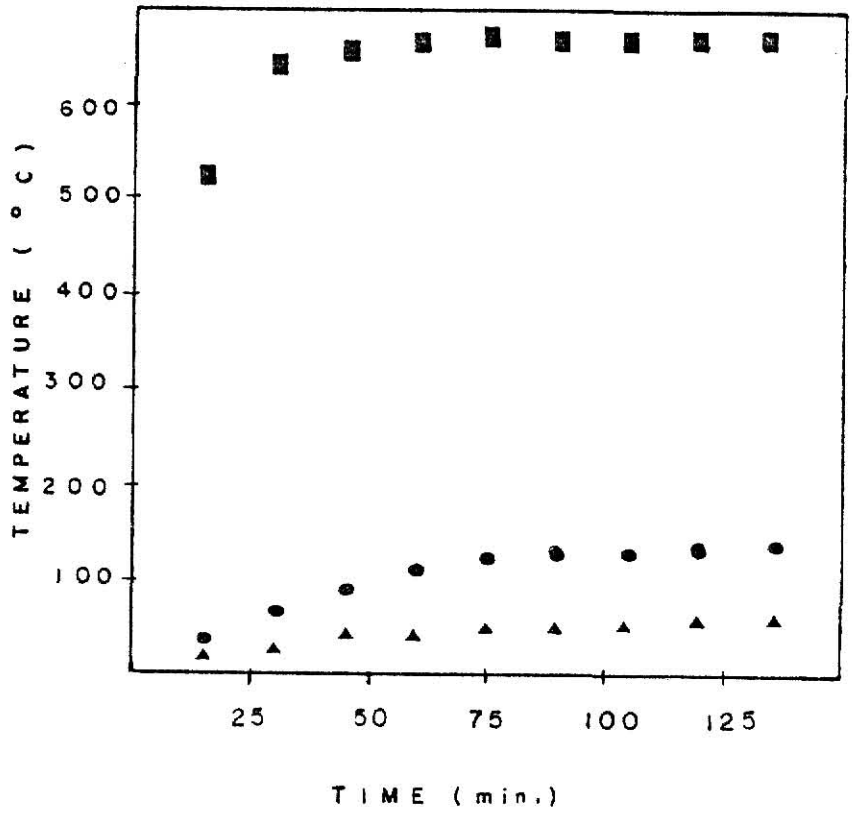

■ Temperature inside specimen chamber

● Temperature at the hot spot

▲ Temperature at the liner

The second preliminary test is a complete series of radiological measurements at various power levels. Additional shielding will be used asnecessary to maintain a reasonable radiation level around the beam port. Calculations of the approximate activities of saturated activation products will be made in order to determine cool down time necessary for removal of experimental equipment. Calculation of the radiolytic gas concentration in the vicinity of the beam port will be completed before any purge gas other than He may be used.

A written procedure will be developed from the preliminary tests and this procedure shall be approved by the Reactor Safeguards Committee.

Procedure of Operation of Electrically Heated Irradiation Chamber in the Radial Piercing Beamport

Purpose: To allow operation of the heater in the electrically heated irradiation chamber as described in Experiment 41 (Reference Experiment 41 of KSU TRIGA Mk. II Reactor).

Procedure:

1. Set the switch (in the box) to the heater in OFF position. Connect all the wiring to the thermocouple and heater (See Fig. 1). Connect the purge gas pipe to the chamber.

2. Adjust the purge gas flowrate to 500 ml/min. (i.e., the scale reads 1.5 on Model 36-541-21 of Fisher Flow meter).

3. Energize the voltmeter, milli-micro voltmeter, and the strip chart recorder. If necessary, adjust the zero reading of all the meters.

4. When the purge gas flow is stable, connect the variable transformer to the line voltage, and turn the heater switch ON. Adjust the voltage gradually until power level is established. The power level must not exceed 200 Watts.

5. Maintain the outer tube thermocouple voltage less than 4 mV.

6. Steps 1 through 5 must be completed at least 15 minutes before reactor start up. Maintain purge gas flow for 30 minutes after the heater is switched off.

7. During insertion and removal of the sample, standard radiological procedures must be used.

   CAUTION: At no time during the heater operation may thermocouple #3 read above 4 mV. If reading 4 mV is obtained, the heater must be shut down and purge flow increased to maximum.

APPENDIX II

Derivation of the Reaction Rate Equation to determine the Therman Neutron Flux Using Bare and Cadmium Covered Foils.

The reaction rate per unit volume in the detector can be expressed as

$$R(E)dE = N_d \, \sigma_a(E) \, \phi(D)dE \quad . \tag{A.II.1}$$

The total reaction rate for energy interval, 0 to ∞, is

$$R = \int_0^\infty R(E)dE = N_d \int_0^\infty \sigma_a(E) \, \phi(E)dE \quad . \tag{A.II.2}$$

The neutron flux in the reactor can be considered to be composed of two group, a thermal group and fast group. The thermal group is defined for those neutrons whose energy is between 0 to 0.2 eV, and the fast group is defined for energy above 0.2 eV. The thermal neutron group exhibits a Maxwell-Boltzmann distribution. If ϕ_{MB} (E) is the neutron flux which have energies between E and E + dE, and $\phi_{th} = \int_0^\infty \phi(E)dE$, then the Maxwell-Boltzmann distribution for thermal neutron flux can be written as

$$\phi_{MB}(E) = \phi_{th} \frac{E}{E_T^2} e^{-E/E_T} \quad , \tag{A.II.3}$$

where

E = neutron energy

E_T = most probable neutron energy at 298 K.

The total thermal neutron flux (ϕ_{th}) can be rewritten as

$$\phi_{th} = \int_0^{\infty} \phi_{MB}(E)dE \simeq \int_0^{E_{TC}} \phi_{MB}(E)dE \quad , \tag{A.II.4}$$

where E_{TC} is the thermal cutoff energy ($\simeq$ 0.2 eV).

For the fast group, i.e., for neutron with energy $E>E_{TC}$, the distribution exhibits a 1/E dependence. The total fast neutron flux can be expressed as

$$\phi_f = \int_{E_{TC}}^{E_{max}} \phi(E)dE \quad , \tag{A.II.5}$$

where E_{max} = maximum energy of neutron $\simeq$20MeV.

Now, if we assume the absorption cross-section of the detecting material exhibits a 1/v dependence which can be expressed as

$$\sigma_a(E) = \sigma_o \frac{\sqrt{E_o}}{\sqrt{E}} \quad , \tag{A.II.6}$$

where σ_o = value at energy E_o ,

and E_o = 0.025eV,

then the total reaction rate is

$$R = N_d \left\{ \int_0^{E_{TC}} \sigma_o \frac{\sqrt{E_o}}{\sqrt{E}} \phi_{MB}(E)dE + \int_{E_{TC}}^{E_{max}} \sigma_a(E)\ \phi(E)dE \right\} \tag{A.II.7}$$

or

$$R = N_d \bar{\sigma} \phi_{th} + N_d \int_{E_{TC}}^{E_{max}} \sigma_a(E)\ \phi(E) dE \quad , \tag{A.II.8}$$

where

$$\bar{\sigma} = \frac{\int_o^\infty \sigma_o \left(\frac{E_o}{E}\right)^{\frac{1}{2}} \phi_{MB}(E) dE}{\int_o^\infty \phi_{MB}(E) dE} \quad ,$$

$$= \left(\frac{\pi}{4} \frac{E_o}{E_T}\right)^{\frac{1}{2}} \sigma_o \quad ,$$

$$= \left(\frac{\pi}{4}\right)^{\frac{1}{2}} \sigma_o(E_T) \quad .$$

To evaluate the reaction for fast neutron group we introduce E_{CC}, which is the effective cadmium cut off energy, (0.4eV) and rewrite the reaction rate for fast neutron groups as

$$R_{fast} = N_d \{ \int_{E_{TC}}^{E_{CC}} \sigma_a(E) \phi(E)\ dE + \int_{E_{CC}}^{E_{max}} \sigma_a(E) \phi(E)\ dE \} \tag{A.II.9}$$

Between energy interval E_{TC} and E_{CC}, $\sigma_a(E)$ can be expressed as

$$\sigma_a(E) = \sigma_o \left(\frac{E_o}{E}\right)^{\frac{1}{2}} \tag{A.II.10}$$

and

$$R_{fast} = N_d \int_{E_{TC}}^{E_{CC}} \sigma_o \left(\frac{E_o}{E}\right)^{\frac{1}{2}} \phi(E)\ dE + N_d \int_{E_{CC}}^{E_{max}} dE\ \sigma_a(E) \phi(E) \tag{A.II.11}$$

The total reaction rate becomes

$$R = N_d \left(\bar{\sigma}\ \phi_{th} + \int_{E_{TC}}^{E_{CC}} \sigma_o \left(\frac{E_o}{E} \right)^{\frac{1}{2}} \phi(E)dE + \int_{E_{CC}}^{E_{max}} \sigma_a(E)\phi(E) \right) \qquad (A.II.12)$$

To measure the thermal neutron flux, the measurement has to be done in two steps. The first step is by irradiating bare foil, which gives the activation due to both thermal and fast neutron. The second step is the radiation of the cadmium covered foil, where the activation is mainly due to the neutron with energies above E_{CC} or mathematically,

$$R_{Cd} = \int_{E_{CC}}^{E_{max}} \sigma_a(E)\phi(E)dE \qquad (A.II.13)$$

The integral expression is called the "resonance integral" of the detector, a quantity which has been measured for a large number of materials. For goil foil the value of the resonance integral is ≃ 1558 barn[20]. From cadmium covered foil, then the value of ϕ_o can be evaluated.

By subtracting the reaction rate measured by the cadmium covered foil from the reaction rate measured by the bare foil, the reaction rate, caused by the thermal neutron flux and a small part of the fast neutron flux is given by

$$R_{th} = R_{bare} - R_{cd} = N_d \left(\bar{\sigma}\phi_{th} + \int_{E_{TC}}^{E_{CC}} \sigma_o \left(\frac{E_o}{E} \right)^{\frac{1}{2}} \phi(E)dE \right) \qquad (A.II.14)$$

Since R_{bare} and R_{cd} are determined from the result of cadmium covered foil, then ϕ_{th} can be determined. In practice, the value of the second term, which is called the activation due to the subcadmium neutron, is much smaller compared to the thermal neutron, and is neglected.

The Correction During Irradiation[20]

Two main corrections during the irradiations are the self shielding correction and the flux perturbations.

a. Self Shielding

During the irradiation, especially for a detector with a large activation cross section, the flux through the foil is not constant. The self-shielding function, $G(\tau)$, is defined as the ratio of the average flux through the volume to the average flux over the surface of the foil

$$G(\tau) = \bar{\phi}_v / \bar{\phi}_s \quad . \tag{A.II.15}$$

The average flux through the volume is related to the activation, c ($cm^{-2}sec^{-2}$), by

$$c = \frac{\tau}{\phi_v} \tag{A.II.16}$$

where

τ = product of foil thickness, t, and the macroscopic activation cross section.

The activation of successive foil layers can be computed by expanding the average surface flux in terms of its angular components, $P_\ell(\cos\Theta)$, with coefficients K_ℓ. The total activation is then the integral over the differential activation of the various layers and summed over all the angular components.

$$c = \sum_{\ell=o}^{\infty} (2\ell+1)K_\ell \int_o^\tau \int_o^\pi p_\ell(\cos\theta)\sin\theta \; \Sigma_a \exp(-x\Sigma_a/\cos\theta) \; d\theta dx \; . \tag{A.II.17}$$

where

Σ_a' is the total absorption cross section. If $\Sigma_a' \simeq \Sigma_a$, the integration gives the self-shielding as

$$G(\tau) = \frac{1}{\tau} \frac{\{[-\frac{1}{2} - E_3(\tau)] \; K_0 + 3 \; [\frac{1}{3} - E_4(\tau)] \; K_1 + \ldots\}}{\int_0^{4\pi} \phi_s(\cos\Theta) \; d\Omega} \tag{A.II.18}$$

where

$$E_n(\tau) = \int_1^\infty \frac{e^{-\tau x}}{x^n} \, dx.$$

For $\tau < 0.05$, the self-shielding can be very closely approximated by

$$G(\tau) = 1 - \tau(1 - \ln \tau). \tag{A.II.19}$$

The self-shielding in the resonance region for a thin foil can be approximated by

$$G_r(\tau) = 1 + \frac{\tau_r \ln \tau_r}{4} - 0.3274 \; \tau_r \tag{A.II.20}$$

where

τ_r = foil thickness times macroscopic absorption cross sections at resonance peak.

b. Flux Perturbation

The flux perturbation, $F(\gamma,\tau)$, is defined as the ratio of the activation of a foil in the perturbed flux, (ϕ_s) to that which would result in an unperturbed flux (ϕ_o)

$$F(\gamma,\tau) = \bar{\phi}_s/\phi_o$$

where

$$\gamma = \Sigma_s/\Sigma_{tot}.$$

$F(\gamma,\tau)$ can be approximated by

$$F(\gamma,\tau) = \{1 + [\frac{1}{2} - E_3(\tau))\ g\ (\gamma,\tau)\}^{-1}$$

where

$g(\gamma,\tau)$ for small foil $(R << \lambda_s\ 1)$ is

$$g(\gamma,\tau) = 9.68\ (R/\lambda_s)$$

where R is radius of foil and λ_s is the scattering mean free path.

c. The Relation Between Measured Activation and Unperturbed Flux

If A_m is the measured activity, and A_o is the activity due to unperturbed flux, then

$$A_m = A_o \left(\frac{\bar{\phi}_v}{\phi_s}\right) \left(\frac{\bar{\phi}_s}{\phi_o}\right)$$

$$= A_o\ G(\tau)\ F(\gamma,\tau)$$

Design and Construction of a Fast Neutron Irradiation Facility for Use at Elevated Temperature

by

Robertus Ismuntoyo

Doktorandus of Physics
Gadjah Mada University, 1967
INDONESIA

AN ABSTRACT OF A MASTER'S THESIS

submitted in partial fulfillment of the
requirement for the degree

MASTER OF SCIENCE

Department of Nuclear Engineering
Kansas State University
Manhattan, Kansas 66506

1981

Abstract

A fast Neutron Irradiation Facility was designed and constructed for the K. S. U. TRIGA Mark II Reactor. It is located in the radial piercing beamport. The temperature in the irradiation chamber can be elevated up to 900 K. Helium was used as a purge gas to transfer heat by convection and to reduce the possibility of oxidation on the sample.

Four measurements were conducted before and during the installation. These were the measurement of the temperature distribution, radiation hazard, the thermal and fast neutron flux, and the irradiation of lithium fluoride. The thermal neutron flux was measured using a gold foil. The fast neutron flux was measuring using three threshold detectors, namely Indium, Nickel, and Aluminum foils. The energy range covered by the threshold detector was 1.4 to 20 MeV.

The lithium fluoride crystal was irradiated at various temperatures, ranging from room temperature up to 773 K. The result from the irradiation of LiF in the gamma cell irradiator was used to estimate the effect of prompt gamma rays from fission.